ADVANCED OPTICAL MATERIALS
www.advopticalmat.de

1521495, 2012, 44, Downloaded from https://onlinelibrary.wiley.com/doi/10.1002/adma.201202624 by Cochrane Russian Federation, Wiley Online Library on [13/02/2023]. See the Terms and Conditions (https://onlinelibrary.wiley.com/terms-and-conditions) on Wiley Online Library for rules of use; OA articles are governed by the applicable Creative Commons License

REVIEW

Invisibility and Cloaking Based on Scattering Cancellation

*Pai-Yen Chen, Jason Soric, and Andrea Alù**

Advances in material synthesis and in metamaterial technology offer new venues to tailor the electromagnetic properties of devices, which may go beyond conventional limits in a variety of fields and applications. Invisibility and cloaking are perhaps one of the most thought-provoking possibilities offered by these new classes of advanced materials. Here, recently proposed solutions for invisibility and cloaking using metamaterials, metasurfaces, graphene and/or plasmonic materials in different spectral ranges are reviewed and highlighted. The focus is primarily on scattering-cancellation approaches, describing material challenges, venues and opportunities for the plasmonic and the mantle cloaking techniques, applied to various frequency windows and devices. Analogies, potentials and relevant opportunities of these concepts are discussed, their potential realization and the underlying technology required to verify these phenomena are reviewed with an emphasis on the material aspects involved. Finally, these solutions are compared with other popular cloaking techniques.

1. Introduction

Recent advances in material science and micro-/nanosynthesis approaches have created large interest in the field of artificial materials and *metamaterials*, formed by suitably engineered inclusions whose collective response may go beyond the limitations of natural materials.[1–5] In metamaterials the average lattice constant is much smaller than the wavelength of operation, and their effective macroscopic properties, such as the electric permittivity and/or magnetic permeability, assume values not commonly available in nature at the frequency of interest. At infrared (IR) and optical frequencies, specific interest has been devoted to novel material platforms for these artificial materials, such as plasmonic nanoparticles, doped semiconductors and graphene, which may interact with electromagnetic waves in anomalous and exotic ways, providing new phenomena and applications. These material platforms have been recently proposed as building blocks for metamaterials, creating interesting new venues in a variety of terahertz (THz), infrared, and optical applications.[6–12]

Metamaterials have attracted a great deal of attention in the media and the general public for the exciting applications enabled by their anomalous physics. A left-handed metamaterial slab, with negative refractive properties, may act as a "perfect lens", which overcomes the intrinsic limits of diffraction in optics and providing subwavelength spatial details at its extended focal plane.[13,14] Subsequent papers have broadened the scope and applicability of these concepts, to realize subdiffractive imaging and sensing, nanolithography, and high-density optical storage.[15,16] The interest in metamaterials has been further fostered by the seminal discovery that metamaterials and/or plasmonic materials may be used to achieve anomalous transparency effects, or "hide" a given object, making it effectively invisible to the electromagnetic radiation.[17–27] This passive camouflaging technique has soon become one of the main attractions for metamaterial applications, with the iconic term of *invisibility cloaking*. Since 2003, cloaking an object by metamaterial and plasmonic structures has been studied in a variety of approaches and applications. In addition to radar detection, defense and military applications, cloaking has been proposed to improve near-field sensors and detectors, such that their presence may cause less disturbance to the environment in sensing networks and systems.[28–34] This "cloaking a sensor" technique may be useful in many setups, e.g., near-field scanning optical microscopes (NSOM) or receiving antennas in a communication network or indoor system.[28–34] Biological and medical research often requires imaging the nanometer-scale details of molecules and nanoparticles,[35] and these subdiffractive measurements are usually performed in the very near field of the object's details to be imaged, being therefore intrinsically limited by the disturbance introduced by the close proximity of the sensing instrument, i.e., a sensing probe that may perturb the near field distributions and influence the measurement.[29] As a result, a "cloaked" sensor with low scattering may significantly improve sensing, detection, near-field measurements, and communication technologies requiring low levels of interference and noise.[28–34]

In recent years, cloaking technology has been developed by several research groups and with different approaches. Theoretically, dramatic scattering suppression may be achieved with specific metamaterials independent of the size of the object and the frequency of operation, but this usually assumes that the required material properties may be realized with a high degree of accuracy in the desired frequency range, which is often not the case. Experimental validations have been realized for different cloaking approaches and in different spectral ranges and even other types of waves, spanning from static[36] and low frequencies[37,38] to microwaves,[39–46] infrared and visible frequencies.[34,47–55]

P.-Y. Chen, J. Soric, Dr. Andrea Alù
The University of Texas at Austin
Department of Electrical and Computer Engineering
1 University Station C0803, Austin, TX, 78712-0240, USA
E-mail: alu@mail.utexas.edu

DOI: 10.1002/adma.201202624

© 2012 WILEY-VCH Verlag GmbH & Co. KGaA, Weinheim

Among the various cloaking approaches, two major categories may be highlighted: *transformation-based metamaterial cloaking* applies the concept of transformation optics and optical conformal mapping,[21,22] whereas *scattering-cancellation-based cloaking*, such as the plasmonic cloaking,[19] and mantle cloaking,[27] focuses on nonresonant destructive interference at all angles. So far, several experimental realizations, applying transformation-based,[37–39,44,47–54] scattering-cancellation-based,[34,36,40,45] transmission-line-based,[42,43] or mirage-effect-based cloaking techniques,[55] have been extended from microwaves to the infrared and visible regimes. Each of these cloaking techniques has their own advantages and constraints, which we discuss in the following sections. In this Review, we particularly focus on scattering cancellation approaches, which provide exciting potentials in several frequency regimes and for different operations. Before describing in detail the various approaches in this category, we review a few other approaches that have been very popular in the recent literature.

2. Metamaterial and Transformation-Based Cloaking

Transformation optics is arguably the most popular tool at present to tailor and manipulate the wave propagation in complex media and metamaterials, providing unprecedented, and in principle unlimited, control, which may be also applied to cloaking. The physical mechanism behind this general approach is based on conformal transformation of coordinates, now popular as "transformation optics". Invisibility cloaking is arguably the most thought-provoking example of transformation optics,[17,20–26] which has been theoretically studied in the ray optics and static limits,[21] and then generalized to dynamic scattering theory.[56] Transformation-based cloaks have been the first to be experimentally realized at microwaves,[39] they have also been implemented at acoustic waves,[37,38] and later extended to infrared and visible frequencies.[47–53] A transformation-based cloak requires anisotropic and inhomogeneous material profiles to distort the isotropic space, rerouting the incoming electromagnetic wave and completely isolating the cloaked region, as if the system is effectively invisible to an external observer.

The cloaking effect is in some sense similar to a mirage effect, in which light rays are bent, displacing images of distant objects, due to temperature gradients in the air layers above the ground and ahead of the observer. In this context, scientists have recently demonstrated that a transparent sheet of highly aligned carbon nanotubes, which possess exceptionally high axial thermal conductivity, may be easily heated to high temperatures, transferring heat to its surrounding areas and causing a steep temperature gradient. Just like a mirage, this steep temperature gradient causes the light rays to bend away from the object concealed behind the cloak, making it effectively invisible.[55]

In their seminal paper,[21] Pendry et al. introduced this cloaking technique and proposed the permittivity and permeability tensor components required for a transformation-based cloak for a spherical object:

Jason C. Soric is a graduate research assistant under the supervision of Dr. Andrea Alù in the Metamaterials and Plasmonics Research Group at the University of Texas at Austin, where he is currently pursuing a Ph.D. in electrical engineering. He received his B.S. and M.S. degrees from the University of Texas at Austin in Electrical Engineering. He was an engineer at Harris Microwave Communications Division in San Antonio, TX, where he was the lead of Tx/Rx ATE bench testing. He has also interned at Ball Aerospace and Technologies Corp. and Raytheon Space and Airborne Systems, where he focused on conformal phased arrays and the near-field testing of AESA radar systems. His research interests include active/passive metamaterials and metasurfaces, small antennas, minimum scattering antennas and sensors, cloaking and invisibility, waveguiding systems, and material characterization.

Pai-Yen Chen was born in Taiwan on September 19, 1982. He received both his B.S. and M.S. in Mechanical Engineering (major) and Electro-optical Engineering from the National Chiao Tung University, Taiwan, in 2004 and 2006, respectively. From 2006 to 2009, he was an Assistant Researcher at the National Nano Device Laboratories (NDL), Taiwan. Since 2009 summer, he is working toward his Ph.D. degree in the Department of Electrical and Computer Engineering, University of Texas in Austin. His doctoral work mainly focuses on nonlinear, passive and active electromagnetic metamaterials and plasmonics, and their RF, THz, infrared and optical applications. He is also actively engaged on graphene and other carbon-based nanoelectronics and nanophotonics.

Andrea Alù is an Assistant Professor at the University of Texas at Austin. He received the *Laurea*, M.S. and Ph.D. degrees from the University of Roma Tre, Rome, Italy, respectively in 2001, 2003, and 2007. From 2002 to 2008, he has been periodically working at the University of Pennsylvania, Philadelphia, PA., where he has also developed significant parts of his Ph.D. and postgraduate research. After spending one year as a postdoctoral research fellow at The University of Pennsylvania, in 2009 he joined the faculty of the University of Texas at Austin. He is also a member of the Applied Research Laboratories and of the Wireless Networking and Communications Group at UT Austin. His current research interests span over a broad range of areas, including metamaterials and plasmonics, electromagnetics, optics and photonics, acoustics, scattering, cloaking and transparency, nanocircuits and nanostructures modeling, miniaturized antennas and nanoantennas, RF antennas and circuits.

© 2012 WILEY-VCH Verlag GmbH & Co. KGaA, Weinheim

15214095, 2012, 44, Downloaded from https://onlinelibrary.wiley.com/doi/10.1002/adma.201202624 by Cochrane Russian Federation, Wiley Online Library on [13/02/2023]. See the Terms and Conditions (https://onlinelibrary.wiley.com/terms-and-conditions) on Wiley Online Library for rules of use; OA articles are governed by the applicable Creative Commons License

21951495, 2012, 44, Downloaded from https://onlinelibrary.wiley.com/doi/10.1002/adma.201202624 by Cochrane Russian Federation, Wiley Online Library on [13/02/2023]. See the Terms and Conditions (https://onlinelibrary.wiley.com/terms-and-conditions) on Wiley Online Library for rules of use; OA articles are governed by the applicable Creative Commons License

$$\varepsilon_{rr} = \mu_{rr} = \frac{a_c}{a_c - a}\frac{(r-a)^2}{r^2},$$
$$\varepsilon_{\theta\theta} = \mu_{\theta\theta} = \frac{a_c}{a_c - a},$$
$$\varepsilon_{\phi\phi} = \mu_{\phi\phi} = \frac{a_c}{a_c - a}, \quad (1)$$

where r, θ, φ are the radial coordinates, a and a_c are the inner and outer radii of the cloak. As already discussed, this approach evidently requires specific profiles of anisotropy and inhomogeneity to work, which are not necessarily easy to tailor in a bulk metamaterial. For this reason, various optimization and simplification steps have been put forward to make this cloak design less ideal, but more practically realizable. A simplified version of (1) with linear rather than parabolic variation of the inhomogeneity profile, has been suggested,[57–59] resulting in an imperfect, but more tractable cloak, which has been successfully demonstrated in microwave experiments.[39] To date, numerous simplification and optimization designs aimed at enhancing the cloaking effectiveness and bandwidth have also been proposed.[57,60]

Figure 1 shows a recent experimental realization of a 2D transformation-based metamaterial cloak.[61] In the figure, a snapshot in time of the measured transverse electric field is given for three different scenarios: Figure 1a a free space measurement of the empty waveguide apparatus; Figure 1b a measurement of the covered conducting cylinder away from the design frequency; and Figure 1c the cloaked cylinder at the design frequency. A typical *rerouting* of the impinging wave around the cylindrical object is clearly visible, which was shown to reduce the scattering cross-section by up to 24%, over a narrow bandwidth of about 2.3%.

One of the important advantages of transformation-based cloaking over scattering-cancellation-based methods, which are discussed later in the paper, relates to the fact that this technique does not have, in principle, a limit on the size of the region to be cloaked. Nonetheless, this property sensibly depends on the precise realization of ideal anisotropy and inhomogeneity profiles as in (1), and realistic frequency dispersion and sensitivity to design variations usually makes the ideal functionality of these cloaks quite difficult to achieve beyond a very narrow bandwidth of operation.[61,62] It is usually only possible to realize these specific material profiles in a stepwise or other approximate way and, as a result, an electrically-large transformation-based cloak becomes very sensitive to these imperfections and approximations, providing an upper limit to the size effectively manageable with this approach.[39] Current experimental realizations for full transformation-based cloaks have been limited to a couple of electrical wavelengths. In addition, most of the theoretical and experimental investigations of this technique have been limited to two-dimensional (2D) geometries for specific polarizations, in order to simplify the stringent requirements on the cloaking design.

With current nanofabrication techniques, several exciting proposals to extend these concepts to the visible range have been put forward in the recent literature. A nonmagnetic optical cloak for a cylindrical geometry using metal-wire inclusions has been proposed,[47,63] easing the pain of realizing graded magnetic metamaterials at optical frequencies. Although the cloaking effect is not perfect and the geometry is limited to 2D, this represents an interesting venue for possible realization in the visible spectrum.

Another category of cloaks based on the transformation optics principles is the "carpet cloaking", which suppresses the scattering produced by a bump or defect on a mirror.[64,65] Since in this case scattering suppression is only limited to the reflected waves, and there is no necessity to suppress the forward scattering, causality limitations are much less stringent and broadband, robust cloaking may be achieved.[66] Recently, a three-dimensional 3D carpet invisibility cloak has been designed and fabricated using dielectric face-centered-cubic (fcc) woodpile photonic crystals,[50] which can effectively tailor the refractive index distribution. Carpet cloaks can provide large bandwidths and work for unpolarized light at optical frequencies. However, these planar carpet cloaks cannot achieve the much more demanding and exciting operation of fully 3D cloaks, which make the objects transparent in all directions.[45]

Transformation cloaks have the property of inherently isolating their core region from the exterior, ideally making the cloaking design independent of the specific object to be cloaked. This property, however, does not enable emerging applications like the "cloaking a sensor" idea described in the introduction, for which an observer or receiving detector inside the cloak may be able to sense the outer world without being visible.[28–34] We will show in the next sections how scattering cancellation cloaks may instead enable this functionality. Their penetrability makes also their operation more robust and broadband than transformation-based cloaks, effectively balancing the price of having to modify, in the general case, the cloak design for the specific object to be cloaked.

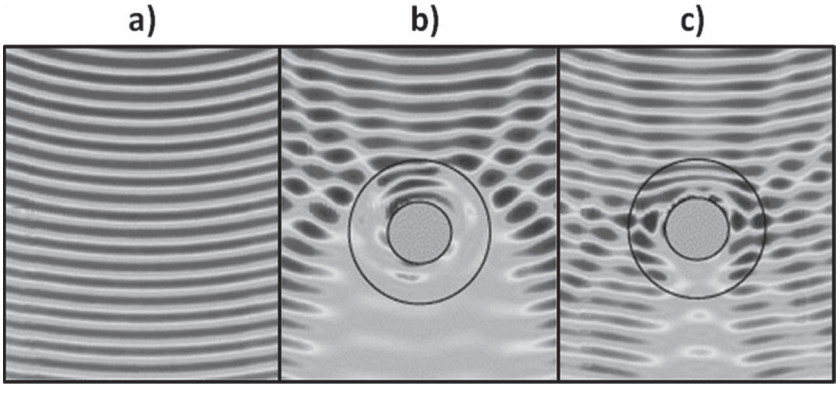

Figure 1. A snapshot of the experimentally measured electric field mapping for (a) no scatterer (10 GHz), and for a covered cylinder (b) away from the cloak's design frequency (9 GHz) and (c) near the cloak's design frequency of operation (10 GHz). Reproduced with permission.[61] Copyright 2010, Institute of Physics.

3. Transmission-Line and Metal-Plate Cloaks

Other exciting venues to cloaking, particularly well suited for radio-frequency (RF)

© 2012 WILEY-VCH Verlag GmbH & Co. KGaA, Weinheim

operation, have been recently put forward in Tretyakov's group in Finland, are in some sense related to the wave rerouting on which transformation-based cloaks are based. The operation of transmission-line (TL) cloaks is straightforward: a properly matched network of receivers (i.e., a circular array of tapered waveguides) couples the incident wave into a mesh of TL networks with minimal reflections.[67] The coupled wavefront is then guided around and through the cloaked region avoiding its interaction with an array of objects placed inside the TL mesh. In this technique, each object to be cloaked must have dimensions fitting inside the unit cell of the TL network. This technique, despite its limitations on the object to be cloaked, may provide very broad bandwidth of operation, and it is particularly well suited for radio-frequencies, in which antennas and transmission-lines are available and well established technology. In this regime, this technique provides wide bandwidth, satisfactory scattering suppression, and ease of fabrication. The operating bandwidth can be considerable, since the phase and group velocities are nearly equal for a properly designed TL network. It has indeed been shown that TL cloaks and plasmonic cloaks may offer considerably larger bandwidth than transformation techniques.[68–71]

In TL cloaks, if the phase velocity inside the cloaked region is less than that of free space, phase matching on the back of the object may be problematic and can introduce disturbances associated to forward scattering, affecting the total scattering suppression. The cloaked region can be realized using microstrip or coaxial circuits, and can be either 2D or 3D. The main disadvantages of TL cloaks consist in its inability to cloak bulk objects, its limits on polarization and its difficult extension to higher frequencies. Moreover, as in the transformation-based cloaking methods, the impinging waves are guided around the cloaked objects, isolating them from the exterior background.

The *metal-plate cloaking* technique has also interesting features, particularly appealing at radio frequencies and recently extended also to infrared and optical frequencies.[43,46,72,73] The cloaked region in this case is surrounded by stacked radial waveguides **Figure 2**a, which are gradually tapered to increase the incident electric and magnetic field concentration towards the edge of the cloaked region. Therefore, the tapered metal plates maintain proper matching to free space for one polarization, due to the roughly constant wave impedance, and gradually decrease the effective index towards the center. The enhanced field concentration eventually creates a circular *channel* around the cloaked region, as simulated in Figure 2b, which, similar to the transformation approach, reroutes the impinging wave and isolates the cloaked region. Although the rerouting functionality of a TL cloak is similar to transformation-based cloaks, its design and operation is much simpler and more robust, and, noticeably, its bandwidth of operation is significantly improved.

Experimental verifications of metal-plate cloaks were presented in two configurations: a 2D (infinite) cylindrical geometry measured in a rectangular waveguide,[43] and a 3D geometry verified by bistatic radar cross-section (RCS) measurements.[46] In both experimental works, a good bandwidth was achieved at microwave frequencies. Also this technique has the evident disadvantage of being strongly sensitive to polarization.

4. Plasmonic Cloaking: From Radio to Optical Frequencies

Plasmonic cloaking is a scattering cancellation technique based on a homogeneous layer with low- or negative- permittivity and/or permeability designed to produce a local polarization vector that is in "anti-phase" with respect to that of the object to be cloaked. Thus, a cancellation between the scattering of the object and of a properly designed plasmonic cover may restore the incident wavefront in the near- and far-field with an operation that is in general independent of the form, polarization and incidence angle of the impinging wave and the position of an observer.[19,39,45,74] Just a single homogeneous plasmonic layer has been shown to significantly suppress the scattering from a few multipolar scattering orders, allowing the cloaking of objects on the scale of the wavelength of operation. Multiband operation and larger objects may be cloaked using multi-layered plasmonic covers, which offer more degrees-of-freedom and allow suppressing a larger number of scattering orders.[75,76]

One key advantage of the plasmonic cloaking technique, attributed to its inherently nonresonant operation, relies on

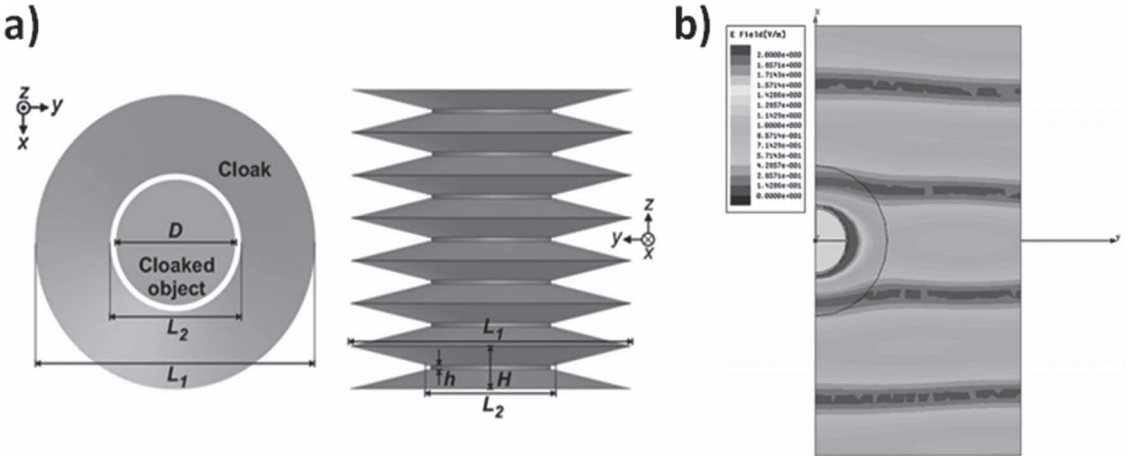

Figure 2. a) Top view (left) and side view (right) of a metal-plate cloak and b) a snapshot of simulated electric fields at the cloak's design frequency (3.2 GHz). Reproduced with permission.[43] Copyright 2009, American Physical Society.

© 2012 WILEY-VCH Verlag GmbH & Co. KGaA, Weinheim

15214095, 2012, 44, Downloaded from https://onlinelibrary.wiley.com/doi/10.1002/adma.201202624 by Cochrane Russian Federation, Wiley Online Library on [13/02/2023]. See the Terms and Conditions (https://onlinelibrary.wiley.com/terms-and-conditions) on Wiley Online Library for rules of use; OA articles are governed by the applicable Creative Commons License

15214095, 2012, 44, Downloaded from https://onlinelibrary.wiley.com/doi/10.1002/adma.201202624 by Cochrane Russian Federation, Wiley Online Library on [13/02/2023]. See the Terms and Conditions (https://onlinelibrary.wiley.com/terms-and-conditions) on Wiley Online Library for rules of use; OA articles are governed by the applicable Creative Commons License

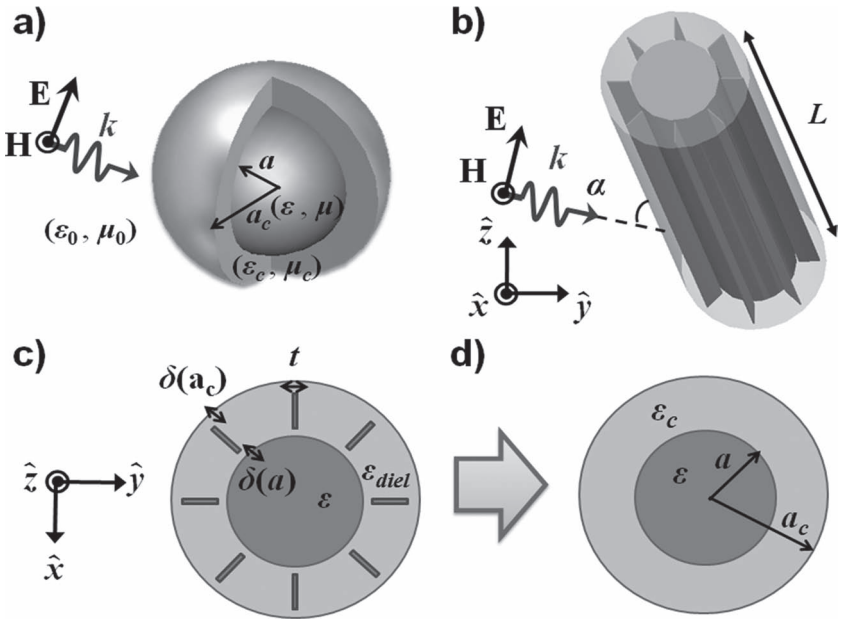

Figure 3. a) cross-section of a magnetodielectric sphere covered by a concentric single-layer shell centered in a suitable spherical reference system (r, θ, ϕ). b) Geometry of a magnetodielectric cylinder covered by a plasmonic shell illuminated in the elevation plane by an obliquely incident plane wave. c) Azimuthal cut of the cylindrical metamaterial cover surrounding a dielectric cylindrical object of permittivity ε, and d) its "homogenized" metamaterial equivalent.

its resiliency to manufacturing tolerances and inherent losses in practical metamaterials. This is often in contrast with transformation-based cloaking techniques,[17–22] which have arguably more sensitivity to frequency, losses and design constraints. Another potential advantage of this technique consists in the possible interaction between the cloaked object and the impinging wave, even as the system is ideally invisible in the electromagnetic fields. For most cloaking techniques, such as transformation-based,[17–22] carpet cloaks,[48–53] transmission-line and metal-plate cloaks,[42,43] the object is usually completely isolated from the incident field. Therefore, despite the fact that these ingenious "conformal mapping" and "rerouting" techniques are able to make the object invisible, inherent to their technique, they cannot be used to sense the external field around them, as in the "cloaking a sensor" application described in the introduction. Scattering cancellation techniques, on the other hand, may be used to improve noninvasive near-field measurements, as well as a multitude of other low-scattering and low-coupling dynamic applications.[28–30] In the following section we review recent progress in plasmonic cloaking.

4.1. Plasmonic Cloaking of Spherical Objects

Consider a magnetiodielectric sphere of radius a, covered by a concentric single-layered plasmonic shell with radius a_c in **Figure 3**a. Here, we assume both the inner sphere and the plasmonic cover to be composed of linear, isotropic and homogenous constitutive parameters (μ, ε) and (μ_c, ε_c), respectively. Both the sphere and the cover may have any real value in the constitutive parameter space and the host medium, while not a requirement, is the one of free space (μ_0, ε_0). Here, we briefly review the conditions for synthesizing a suitable plasmonic cloak that can significantly reduce the total scattering cross-section (SCS) of a magnetiodielectric sphere.[19] We consider time-harmonic constitutive parameters with $e^{-i\omega t}$ time convention, and the covered sphere is illuminated by an impinging monochromatic plane wave $\hat{x}\, E_0 \exp[i\,(k_0 z - \omega t)]$. Following the well-known Lorenz-Mie scattering theory, the incident plane wave may be expressed as a superposition of orthogonal spherical harmonics:[77]

$$\mathbf{E}_i = \sum_{n=1}^{\infty}\sum_{m=-n}^{n} a_{nm}\nabla\times\nabla\times\left(\mathbf{r}\psi_n^m\right) + i\omega\mu_0\sum_{n=1}^{\infty}\sum_{m=-n}^{n} b_{nm}\nabla\times\left(\mathbf{r}\psi_n^m\right),$$

$$\mathbf{H}_i = \sum_{n=1}^{\infty}\sum_{m=-n}^{n} b_{nm}\nabla\times\nabla\times\left(\mathbf{r}\psi_n^m\right) - i\omega\varepsilon_0\sum_{n=1}^{\infty}\sum_{m=-n}^{n} a_{nm}\nabla\times\left(\mathbf{r}\psi_n^m\right). \quad (2)$$

The impinging plane wave may be now expanded into its transverse-magnetic (TM^r) and transverse-electric (TE^r) multipoles with expansion coefficients a_{nm}, b_{nm} of order (n,m), respectively.[77] The spherical harmonics ψ_n^m are eigenmodal solutions to the scalar Helmholtz equation, and $\mathbf{r}$ is the radial position vector, centered at the origin of the core–shell configuration. Similarly, the scattered fields can be expressed as

$$\mathbf{E}_s = \sum_{n=1}^{\infty}\sum_{m=-n}^{n} c_{nm}^{TM} a_{nm}\nabla\times\nabla\times\left(\mathbf{r}\psi_n^m\right) + i\omega\mu_0\sum_{n=1}^{\infty}\sum_{m=-n}^{n} c_{nm}^{TE} b_{nm}\nabla\times\left(\mathbf{r}\psi_n^m\right),$$

$$\mathbf{H}_s = \sum_{n=1}^{\infty}\sum_{m=-n}^{n} c_{nm}^{TE} b_{nm}\nabla\times\nabla\times\left(\mathbf{r}\psi_n^m\right) - i\omega\varepsilon_0\sum_{n=1}^{\infty}\sum_{m=-n}^{n} c_{nm}^{TM} a_{nm}\nabla\times\left(\mathbf{r}\psi_n^m\right), \quad (3)$$

where c_{nm}^{TM} and c_{nm}^{TE} are the scattering coefficients for each scattering multipole. By enforcing the proper continuity of the tangential electric and magnetic fields at the interfaces $r = a$ and $r = a_c$, the scattering coefficients c_{nm}^{TM} and c_{nm}^{TE} can be compactly written as

$$c_{nm}^{\mathrm{TM}} = -\frac{U_n^{\mathrm{TM}}}{U_n^{\mathrm{TM}} + i\,V_n^{\mathrm{TM}}},$$

$$c_{nm}^{\mathrm{TE}} = -\frac{U_n^{\mathrm{TE}}}{U_n^{\mathrm{TE}} + i\,V_n^{\mathrm{TE}}}, \quad (4)$$

where U_n^{TM} and V_n^{TM} are given by

© 2012 WILEY-VCH Verlag GmbH & Co. KGaA, Weinheim

$$U_n^{TM} = \begin{vmatrix} j_n(ka) & j_n(k_c a) & y_n(k_c a) & 0 \\ [ka\, j_n(ka)]'/\varepsilon & [k_c a\, j_n(k_c a)]'/\varepsilon_c & [k_c a\, y_n(k_c a)]'/\varepsilon_c & 0 \\ 0 & j_n(k_c a_c) & y_n(k_c a_c) & j_n(k_0 a_c) \\ 0 & [k_c a_c j_n(k_c a_c)]'/\varepsilon_c & [k_c a_c\, y_n(k_c a_c)]'/\varepsilon_c & [k_c a_c\, j_n(k_0 a_c)]'/\varepsilon_0 \end{vmatrix},$$

and

$$V_n^{TM} = \begin{vmatrix} j_n(ka) & j_n(k_c a) & y_n(k_c a) & 0 \\ [ka j_n(ka)]'/\varepsilon & [k_c a\, j_n(k_c a)]'/\varepsilon_c & [k_c a\, y_n(k_c a)]'/\varepsilon_c & 0 \\ 0 & j_n(k_c a_c) & y_n(k_c a_c) & y_n(k_0 a_c) \\ 0 & [k_c a_c j_n(k_c a_c)]'/\varepsilon_c & [k_c a_c\, y_n(k_c a_c)]'/\varepsilon_c & [k_c a_c\, y_n(k_0 a_c)]'/\varepsilon_0 \end{vmatrix}. \quad (5)$$

Here, $j_n(\cdot)$and $y_n(\cdot)$ are respectively the spherical Bessel functions of the first and second kinds of order n.[78] The wavenumbers in each of the regions are described by their respective constitutive parameters as $k \equiv \omega\sqrt{\varepsilon\mu}$, $k_c \equiv \omega\sqrt{\varepsilon_c\mu_c}$, and $k_0 \equiv \omega\sqrt{\varepsilon_0\mu_0}$. Owing to the symmetry of the core–shell geometry under study in Figure 3a, the azimuthal poles need not be considered here, and the orders m are therefore suppressed in (Equations (2)–(5)). By electromagnetic duality, the scattering coefficients c_{nm}^{TE} can be readily obtained by replacing ε with μ in Equation (5).

Considering a conventional dielectric sphere, Equation (4) presents two interesting scenarios: (1)$V_n^{\mathrm{TM}} = 0$ associated with $c_n^{\mathrm{TM}} = -1$ and resonant scattering, and (2) $U_n^{\mathrm{TM}} = 0$ associated with $c_n^{\mathrm{TM}} = 0$ and zero scattering for the specific scattering order. The former condition physically prescribes a way to dramatically *enhance* the given scattering order.[19] The second condition, on the contrary, may achieve *scattering suppression* of the nth order multipole, which is crucial for realizing nearly-zero scattering and ideally invisibility.[19] It is worth mentioning in this context that, due to the oscillatory nature of the Bessel functions involved in Equation (5), naturally each scattering coefficient hits the conditions for resonance and cloaking as the electrical size increases. However, when the zero of one scattering order is hit, several other orders contribute to the visibility of the object and sharp cloaking or resonant features do not generally arise when conventional materials are considered. By properly manipulating the core–shell electromagnetic properties and considering suitably tailored metamaterial shells, we may be able to align the zeros of all the relevant scattering orders and drastically suppress the overall visibility. In order to achieve this goal, materials with permittivity and/or permeability near zero are usually most effective. Since these properties are commonly available near the effective plasma frequency of the materials, this scattering cancellation technique assumes the name of "plasmonic cloaking".

The total SCS,[79] typically used to fully characterize the contribution of all the scattering coefficients, independent of the form of the impinging wave and of the observer's position, is given by

$$\sigma_{3D} = \frac{2\pi}{|k_0|^2}\sum_{n=1}^{\infty}\sum_{m=-n}^{n}(2n+1)\left(\left|c_{nm}^{TM}\right|^2 + \left|c_{nm}^{TE}\right|^2\right). \quad (6)$$

In the quasistatic limit $k_0 a$, $k_c a_c << 1$, the condition for suppressing the desired scattering harmonic (i.e., $U_n^{\mathrm{TM}} = 0$) can be derived by first-order Taylor expansion of Equation (5):[19]

$$\mathrm{TM}: \frac{a}{a_c} = \sqrt[2n+1]{\frac{(\varepsilon_c - \varepsilon_0)\left[(n+1)\,\varepsilon_c + n\varepsilon\right]}{(\varepsilon_c - \varepsilon)\left[(n+1)\,\varepsilon_c + n\varepsilon_0\right]}}. \quad (7)$$

Equation (7) explicitly delineates the conditions for canceling the nth multipolar order in the quasistatic limit, which depends on the permittivity of the object and cover and the ratio of object-shell radii in the quasistatic limit. For an electrically-small dielectric sphere, the scattering is mainly dominated by c_1^{TM}, related to a distinct dipolar scattering behavior. It may be verified that for a moderate-size dielectric sphere with radius $a < \lambda_0/5$, significant scattering reduction can be achieved with a single plasmonic layer, which is specifically designed to suppress the scattering coefficient c_1^{TM}. In this case, Equation (7) reduces to:[19]

$$\frac{a}{a_c} = \sqrt[3]{\frac{(\varepsilon_c - \varepsilon_0)\,(2\varepsilon_c + \varepsilon)}{(\varepsilon_c - \varepsilon)\,(2\varepsilon_c + \varepsilon_0)}}. \quad (8)$$

In general, the permittivity of the core and shell should be opposite in sign,[19] namely a shell with negative permittivity is necessary to cloak a dielectric object. There is also a compromise between the thinness of the covering shell and the magnitude of its constitutive parameters (i.e., $\mathrm{Re}[\varepsilon_c]$). Scattering suppression can also be achieved by using low-permittivity covers (i.e., $0 < \varepsilon_c < 1$). In fact, low-permittivity covers can be used to strongly reduce the total SCS of a conducting sphere, under the condition:[19]

$$\frac{a}{a_c} = \sqrt[3]{\frac{\varepsilon_0 - \varepsilon_c}{2\varepsilon_c + \varepsilon_0}}. \quad (9)$$

As the size of the sphere becomes larger, additional multipoles are excited and contribute more significantly to the total SCS in Equation (6). For larger spherical objects, the second dominant contribution to the overall scattering is the c_1^{TE} harmonic, corresponding to magnetic dipole radiation; therefore, conditions for the cancellation of the TE multipoles (i.e., $U_n^{\mathrm{TE}} = 0$) are also cast, similar to Equation (7):[19]

$$\mathrm{TE}: \begin{cases} \frac{a}{a_c} = \sqrt[2n]{\frac{(\varepsilon_c - \varepsilon_0)(\varepsilon_c + \varepsilon)}{(\varepsilon_c - \varepsilon)(\varepsilon_c + \varepsilon_0)}} & \text{for } n \neq 0, \\ \frac{a}{a_c} = \sqrt{\frac{\mu_c - \mu_0}{\mu_c - \mu}} & \text{for } n = 0. \end{cases} \quad (10)$$

For larger spherical objects, one can tailor two or more plasmonic shells to reduce the dominant scattering terms, being due to either c_n^{TM} or c_n^{TE}. Even though the physical size of a spherical object is increased by using these covers, which intuitively should increase the total SCS of the shell–core system in Figure 3a, strong scattering suppression is indeed possible, due to the anomalous polarization properties of plasmonic materials. We also note that, by using a single-layer plasmonic cloak composed of metamaterials in which both permittivity and permeability may be controlled at the same design frequency, cancellation of both dominant c_1^{TM} and c_1^{TE} terms may be

© 2012 WILEY-VCH Verlag GmbH & Co. KGaA, Weinheim

15214095, 2012, 44, Downloaded from https://onlinelibrary.wiley.com/doi/10.1002/adma.201202624 by Cochrane Russian Federation, Wiley Online Library on [13/02/2023]. See the Terms and Conditions (https://onlinelibrary.wiley.com/terms-and-conditions) on Wiley Online Library for rules of use; OA articles are governed by the applicable Creative Commons License

15214095, 2012, 44, Downloaded from https://onlinelibrary.wiley.com/doi/10.1002/adma.201202624 by Cochrane Russian Federation, Wiley Online Library on [13/02/2023]. See the Terms and Conditions (https://onlinelibrary.wiley.com/terms-and-conditions) on Wiley Online Library for rules of use; OA articles are governed by the applicable Creative Commons License

achieved.[19,80] Therefore, the residual scattering is contributed by higher-order multipoles, leading to a much reduced total SCS in the case of a moderately sized objects. Finally, we note that this scattering cancellation effect is naturally nonresonant, which makes it quite robust to the frequency of operation, as well as the presence of losses and design imperfections.[81]

4.2. Plasmonic Cloaking of Cylindrical Objects

4.2.1. Theoretical Analysis

In several practical applications, especially in the radar community, 2D geometries and elongated objects may be of particular interest for cloaking applications. Similar to the spherical geometry and analogous to Equations (7)–(10), suitably chosen geometrical and electromagnetic properties of plasmonic covers may realize significant scattering suppression in the case of an infinite cylinder.[74] Here, we consider a general model for cylindrical objects, which includes the effects of arbitrary incidence angle, and which may be applied to cloaking of 3D elongated objects.[45] In this case, we consider an oblique plane wave impinging on a coated infinite cylinder at an angle α (Figure 3b). The radii of core and shell are a and a_c, respectively, and the electric and magnetic properties are given in each region with the same parameters used in the previous section. The scattering coefficients can be written similar to Equation (4),[74] with determinants

$$P_n^{\mathrm{TM}} = \begin{vmatrix} J_n\left(k^T a\right) & J_n\left(k_c^T a\right) & Y_n\left(k_c^T a\right) & 0 \\ \frac{k}{\eta k^T} J_n'\left(k^T a\right) & \frac{k_c}{\eta_c k_c^T} J_n'\left(k_c^T a\right) & \frac{k_c}{\eta_c k_c^T} Y_n'\left(k_c^T a\right) & 0 \\ 0 & J_n\left(k_c^T a_c\right) & Y_n\left(k_c^T a_c\right) & J_n\left(k_0^T a_c\right) \\ 0 & \frac{k_c}{\eta_c k_c^T} J_n'\left(k^T a_c\right) & \frac{k_c}{\eta_c k_c^T} J_n'\left(k_c^T a_c\right) & \frac{k_0}{\eta_0 k_0^T} J_n'\left(k_0^T a_c\right) \end{vmatrix},$$

and

$$Q_n^{\mathrm{TM}} = \begin{vmatrix} J_n\left(k^T a\right) & J_n\left(k_c^T a\right) & Y_n\left(k_c^T a\right) & 0 \\ \frac{k}{\eta k^T} J_n'\left(k^T a\right) & \frac{k_c}{\eta_c k_c^T} J_n'\left(k_c^T a\right) & \frac{k_c}{\eta_c k_c^T} Y_n'\left(k_c^T a\right) & 0 \\ 0 & J_n\left(k_c^T a_c\right) & Y_n\left(k_c^T a_c\right) & Y_n\left(k_0^T a_c\right) \\ 0 & \frac{k_c}{\eta_c k_c^T} J_n'\left(k^T a_c\right) & \frac{k_c}{\eta_c k_c^T} J_n'\left(k_c^T a_c\right) & \frac{k_0}{\eta_0 k_0^T} Y_n'\left(k_0^T a_c\right) \end{vmatrix}. \quad (11)$$

where $J_n(\cdot)$ and $Y_n(\cdot)$ are cylindrical Bessel and Neumann functions of order n,[78] respectively. The characteristic impedance $\eta_l = \sqrt{\mu_l/\varepsilon_l}$ and wavenumber k_l are defined for each region l. Oblique incidence arises in the expression of the transverse wavenumber $k_l^T = \sqrt{k_l^2 - \beta^2}$, where $\beta = k_0 \cos(\alpha)$. Similar to the spherical case, the scattering coefficients c_n^{TM} are written in terms of Equation (11), and c_n^{TE}, associated to TE-polarized cylindrical harmonics, can be obtained by electromagnetic duality. Also in this case, cloaking may be achieved by enforcing $U_n^{\mathrm{TM}} = 0$ and/or $U_n^{\mathrm{TE}} = 0$ and, as a quantitative measure of the cloak's ability to significantly reduce the scattering of a cylindrical object, we consider the total scattering width (SW)[79]

$$\sigma_{2D} = \frac{4}{k_0} \sum_{n=-\infty}^{\infty} \left|c_n^{\mathrm{TM}}\right|^2 + \left|c_n^{\mathrm{TE}}\right|^2. \quad (12)$$

In the long-wavelength limit $k_0 a,\ k_c a_c \ll 1$, the scattering coefficients in Equation (11) are uncoupled and weakly dependent on the angle of incidence. Therefore, akin to the conditions in Equations (7) and (10),[74] scattering cancellation of the dominant scattering multipoles for magnetodielectric cylinders can be written as

$$\begin{aligned} c_0^{\mathrm{TM}} &: \frac{a_c}{a} = \sqrt{\frac{\varepsilon_c - \varepsilon}{\varepsilon_c - \varepsilon_0}}, \\ c_{n\neq 0}^{\mathrm{TM}} &: \frac{a_c}{a} = \sqrt[2n]{\frac{\left(\mu_c - \mu\right)\left(\mu_c + \mu_0\right)}{\left(\mu_c - \mu_0\right)\left(\mu_c + \mu\right)}}, \\ c_0^{\mathrm{TE}} &: \frac{a_c}{a} = \sqrt{\frac{\mu_c - \mu}{\mu_c - \mu_0}}, \\ c_{n\neq 0}^{\mathrm{TE}} &: \frac{a_c}{a} = \sqrt[2n]{\frac{\left(\varepsilon_c - \varepsilon\right)\left(\varepsilon_c + \varepsilon_0\right)}{\left(\varepsilon_c - \varepsilon_0\right)\left(\varepsilon_c + \varepsilon\right)}}. \end{aligned} \quad (13)$$

Cloaking of thin perfect electric conducting (PEC) or conducting cylinders is more challenging than conducting spheres. The reason is that the dominant scattering coefficient c_0^{TM} cannot be cancelled in the quasistatic limit due to the induced axial conduction currents. Nevertheless, significant reduction of all other scattering terms can be achieved by properly choosing the plasmonic cover constitutive parameters and thickness to cancel the subsequent multipolar terms. Under the quasistatic limit, these conditions are given by[74]

$$\begin{aligned} c_0^{\mathrm{TE}} &: \frac{a_c}{a} = \sqrt{\frac{\mu_c}{\mu_c - \mu_0}}, \\ c_{n\neq 0}^{\mathrm{TE}} &: \frac{a_c}{a} = \sqrt[2n]{\frac{\varepsilon_c + \varepsilon_0}{\varepsilon_0 - \varepsilon_c}}, \\ c_{n\neq 0}^{\mathrm{TM}} &: \frac{a_c}{a} = \sqrt[2n]{\frac{\mu_c + \mu_0}{\mu_c - \mu_0}}. \end{aligned} \quad (14)$$

Notice that Equation (14) requires the use of a magnetic permittivity cover to cancel the most significant scattering terms, other than c_0^{TM}, in the quasistatic limit. However, it is important to note here that the cancellation of the dominant c_0^{TM} scattering term may be possible for a thin PEC cylinder, but the cover composition and thickness solution space must be studied using the full dynamic equations in Equation (11) rather than under the quasistatic limit.

Cloaking of cylindrical or other anisotropically-shaped objects presents other challenges: inherent polarization coupling arises for oblique illumination and when considering finite length and low conductivity, additional axial resonances usually arise, which may affect the overall cloaking performance.[74,82,83] However, for thin cylindrical objects with large aspect ratios, the scattering coefficients in Equation (11) are virtually uncoupled and are only weakly affected by oblique excitation.[74]

© 2012 WILEY-VCH Verlag GmbH & Co. KGaA, Weinheim

We have previously shown[74] that, by using a single-layered plasmonic cloak, significant scattering reduction may be obtained for long dielectric cylinders with cross-sections up to a half wavelength, and the scattering suppression is still quite promising up to one wavelength. Properly designed plasmonic cloaks provide significant scattering suppression even for large obliquely incident angles and arbitrary polarization. It is noted that, while the relative reduction of scattering may be less at near-grazing angles than for normal incidence, this is not necessarily relevant, since the strongest scattering occurs at normal incidence for parallel polarization.

4.2.2. Metamaterial Design and Experimental Realization

A number of experimental cloaking verifications have been recently reported for cylindrical targets. Yet these approaches have been usually limited to 2D environments or to reducing the scattering only over a limited angular spectral range, such as in the case of bumps on a mirror or a ground plane (as in the carpet cloaking technique).[37–44,46–53] Photothermal deflection, utilizing the *mirage effect*, has also been shown as an alternative venue to suppress the scattering for specific positions of the observer.[55] We recently reported the first 3D demonstration of metamaterial cloaking in free-space, applicable to arbitrary excitation angle and observer's position, by applying the plasmonic cloaking approach.[45] A metamaterial design at microwave frequencies has confirmed that a single-layer plasmonic shell can drastically reduce the total SCS of a finite-length, moderate-size, dielectric cylinder by suppressing the dominant c_0^{TM} multipole.[45] The realized 3D plasmonic cloak was particularly attractive due to its ease of fabrication, relative invariance to near-grazing incidence, and minor deviation in performance compared to an infinite cylinder.[74] Additionally, since the scattering cancellation mechanism is inherently nonresonant, it has proved quite tolerant to fabrication imperfections and Ohmic losses.

It is well known that natural materials, such as noble metals and some semiconductors at infrared and visible frequencies show Drude-type dispersions due to atomic and electronic transitions at higher energy.[79] To implement a realistic Drude-like metamaterial at lower frequencies,[84] a cylindrical structure composed of N metallic implants embedded in a host dielectric $\varepsilon_{\mathrm{diel}}$, as illustrated in Figure 3c, when excited with electric field parallel to the $\hat{\mathbf{z}}$ axis, provides the effective permittivity

$$\varepsilon_{\mathrm{eff}} \approx \varepsilon_{\mathrm{diel}} - \frac{N^2 \varepsilon_0}{4k_0^2 a a_c}. \tag{15}$$

As illustrated in Figure 3c,d, a properly designed cylindrical metamaterial cover can be homogenized as an equivalent bulk material of permittivity given by Equation (15). By selecting the number of metallic implants, inner and outer radii, and the host dielectric, we may be able to tailor the required effective permittivity over a large range of values. In the practical design, the number of metallic implants cannot be too small, since this may also reduce the effectiveness and isotropy of the metamaterial. Also, the metamaterial disc should be fairly thin compared to the operating wavelength, since unwanted resonances may appear across the host dielectric region $a_c - a$ for large cover thicknesses, especially for a large dielectric constant of the filling material $\varepsilon_{\mathrm{diel}}$.[85] In addition, a small gap needs to be considered at each of the interfaces $r = a$ and $r = a_c$:[84]

$$\delta(r) \approx 0.1 \frac{2\pi}{N} r, \tag{16}$$

where r is the radial distance relative to the cylinder center. These recommended "virtual interfaces" in Equation (16) allow sufficient distance to neglect the effects of evanescent Floquet modes at the disc interface. These concepts were put forward and verified numerically[74,84] and later, demonstrated by the first experimental 2D plasmonic cloak[40] and experimental 3D plasmonic cloak.[45]

Here, we provide a few numerical full-wave simulations, using CST Microwave Studio,[86] with the aim of validating the effectiveness of this plasmonic cloaking technique for finite-length, moderate-size, dielectric cylinders in free space. We use the same cloak design as our recent experimental paper,[45] but we provide here additional numerical and experimental results, providing further physical insights into its functionality. The metamaterial-assembled plasmonic cloak was designed to significantly reduce the scattering of a dielectric cylinder of length $L = 1.8\lambda_0$ and diameter $2a = \lambda_0/4$, where λ_0 is the free space wavelength at the design frequency $f_0 = 3$ GHz. The length of the dielectric object was chosen to be about two wavelengths, which may induce axial resonances especially in the case of oblique illumination and TM^z polarization.[45] The dielectric cylinder has constitutive parameters $(3\varepsilon_0, \mu_0)$ and we consider realistic dielectric losses with $\tan\delta = 0.002|_{3\ \mathrm{GHz}}$. A plasmonic cylindrical cloak is designed, following the model of Figure 3, for TM^z impinging wave (with electric field polarized parallel to the cylinder axis) at normal incidence, which produces the largest total SCS. The cloak is tuned to cancel the dominate scattering multipole c_0^{TM}, which dominates the total SCS for these dimensions. To avoid the excitation of higher-order resonances across the shell thickness $a_c - a$, a conformal plasmonic cover of $a_c/a \simeq 1.3$ was implemented. The metal assumed for the metallic implants is copper, with finite conductivity $\sigma_{\mathrm{Cu}} = 5.8 \times 10^7 \mathrm{S/m}$.

In order to suppress the dominant dipolar scattering, the required effective permittivity of the plasmonic shell is $\varepsilon_c = -13.6\varepsilon_0$, in accordance with (7). To achieve this permittivity value, a conformal metamaterial cloak was implemented with $N = 8$ vertical metallic strips, which are inserted into a filling dielectric of $\varepsilon_{\mathrm{diel}} = 16\varepsilon_0$ of thickness $a_c - a = 0.0375\lambda_0$. The number of vertical metallic strips was necessary to maintain the isotropy of plasmonic shell, while maintaining a relatively low filling dielectric. Additionally, the radial length of the metallic fins was designed according to Equation (16) to obviate the effects of evanescent Floquet modes at the two radial interfaces.

Figure 4 shows full-wave simulations comparing the scattering of the uncloaked (Figure 4a) and cloaked (Figure 4b) dielectric cylinders in the azimuthal plane at the design frequency, when excited by a plane wave propagating along the $-\hat{x}$ axis, with electric field polarized along the $\hat{z}$ axis. The near-field field distribution of the cloaked object Figure 4b shows that the phase front of the impinging plane wave is almost completely restored even just outside the cloak, and higher-order scattering

© 2012 WILEY-VCH Verlag GmbH & Co. KGaA, Weinheim

15214095, 2012, 44, Downloaded from https://onlinelibrary.wiley.com/doi/10.1002/adma.201202624 by Cochrane Russian Federation, Wiley Online Library on [13/02/2023]. See the Terms and Conditions (https://onlinelibrary.wiley.com/terms-and-conditions) on Wiley Online Library for rules of use; OA articles are governed by the applicable Creative Commons License

15214095, 2012, 44, Downloaded from https://onlinelibrary.wiley.com/doi/10.1002/adma.201202624 by Cochrane Russian Federation, Wiley Online Library on [13/02/2023]. See the Terms and Conditions (https://onlinelibrary.wiley.com/terms-and-conditions) on Wiley Online Library for rules of use; OA articles are governed by the applicable Creative Commons License

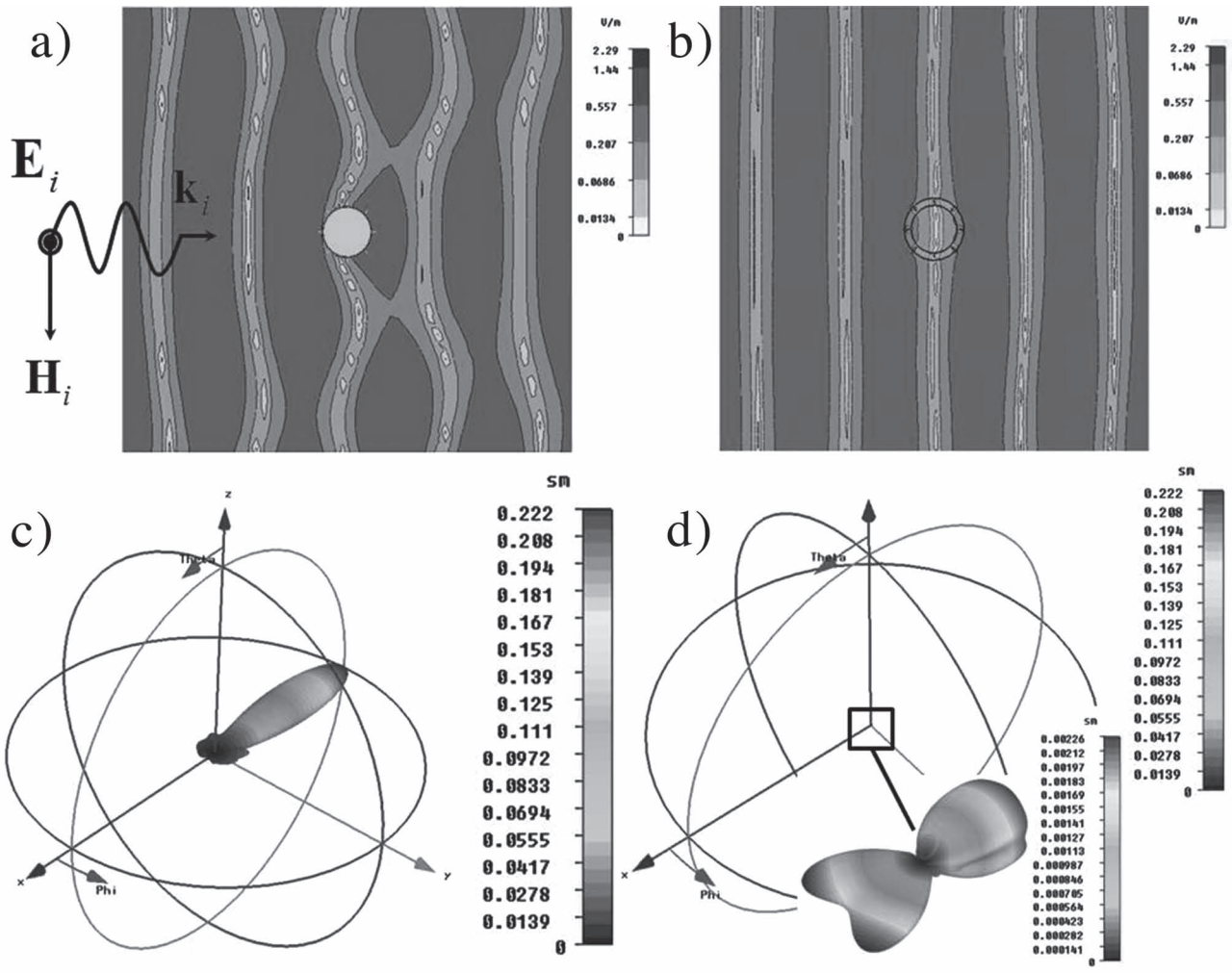

Figure 4. Near-field snapshot in time of the TM-polarized electric field distribution in the azimuthal plane of: a) the uncloaked cylinder, b) the cloaked object. Far-field total SCS of the c) uncloaked, and d) cloaked object with zoomed-in view at 3.13 GHz. These results have been obtained with full-wave simulations.

coefficients contribute very little to the overall residual scattering. The total SCS far-field pattern of the cloaked cylinder in Figure 4d shows a dramatic reduction compared to the uncloaked case Figure 4c, close to 12 dB at 3.13 GHz. The pattern of the uncloaked dielectric cylinder shows a large forward scattering (shadow), which is almost completely suppressed when covered by the plasmonic cloak. In Figure 4d, the residual scattering (zoomed in to see it in a different scale) shows minimal higher-order multipole contributions. It is important to point out that losses were considered in the simulations of Figure 4, and there is clearly no significant detrimental effect on the cloaking performance, which further demonstrates the robustness of this scattering-cancellation technique.

Next, we show in **Figure 5** the frequency dispersion of three significant scattering metrics: total SCS, forward-, and backscattering cross-sections of the cloaked object normalized to the uncloaked one.[79] The normalized total SCS shows a relevant scattering reduction over a relatively broad bandwidth $\mathrm{BW} = \Delta f_{0\,\mathrm{dB}}/f_{\mathrm{center}} = 14.7\%$, defined as the fractional bandwidth over which the total scattering is reduced compared to the

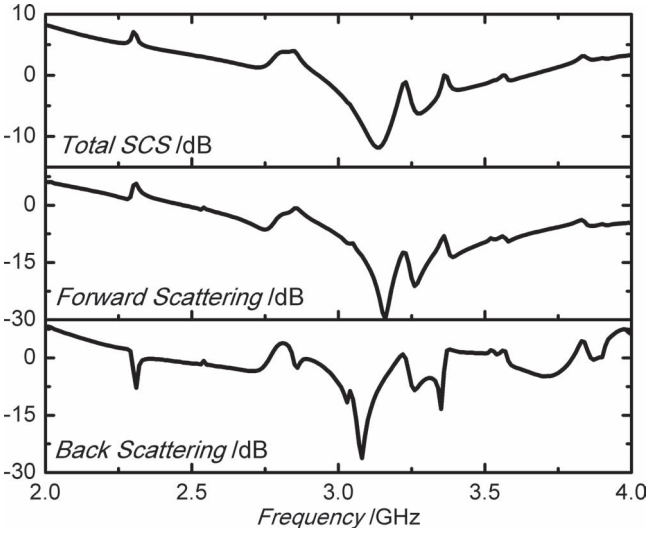

Figure 5. Full-wave simulations for the total, forward, and backscattering cross-section of the cloaked object normalized to the uncloaked cylinder.

© 2012 WILEY-VCH Verlag GmbH & Co. KGaA, Weinheim

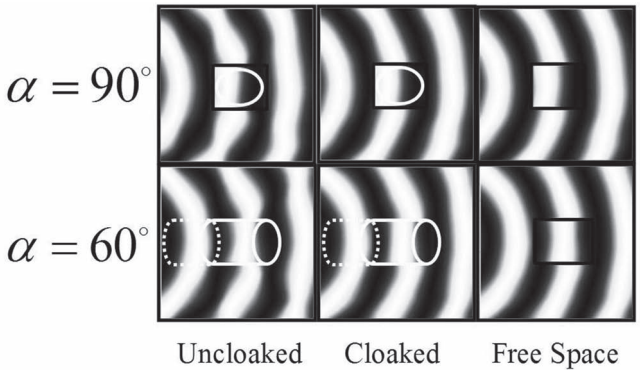

Figure 6. Snapshots in time of the uncloaked object, cloaked object, and free space near-field measurements (S_{21}) at 3.13 GHz for normal (90°) and oblique (60°) incidence angles, where α is measured from the $\hat{\mathbf{z}}$ axis, referring to the geometry in Figure 3c.

uncloaked object. Distinct SCS dips are observed for all three cases. For the back-scattering, a slight shift in dip position and narrower BWs are obtained. The main reason of this apparent bandwidth reduction is that the back-scattering is already quite low for an uncloaked dielectric object, as most of the scattering is in the forward direction (shadow). Very impressive scattering suppression is indeed found in the forward direction, ensuring much reduced shadow from the cylindrical object.

The metamaterial shell in Figure 4 was recently fabricated and measured in both the near-field and far-field regions to characterize its scattering profile in 3D.[45] The host dielectric was assembled by separate sectoral pieces of Cuming Microwave C-Stock dielectric material,[87] and the vertical metallic implants were made from precisely cutting copper tape strips with 66.0 μm thickness. The dielectric sectors are held together by Teflon end caps, which showed no significant change in the cloak operation. The "virtual interfaces" were optimized for $\delta(a) = 0.98$ mm and $\delta(a_c) = 1.3$ mm. We present here the measured scattering profiles in the near-field of the uncloaked and cloaked dielectric cylinders at the cloaking frequency, as shown in **Figure 6**, when illuminated by a Gaussian beam produced by a horn antenna placed in the near-field of the objects. Each one of the targets is also compared to wave propagation in free space (i.e., the test environment without any object). Figure 6 shows the total near-field distribution for normal ($\alpha = 90°$) and oblique incidence ($\alpha = 60°$). In each near-field panel, the scan area in the y–z plane is a square azimuthal cut of $2.16\lambda_0 \times 2.16\lambda_0$ for normal incidence, and $3.10\lambda_0 \times 3.10\lambda_0$, for oblique incidence, with equal step sizes of $\Delta y = \Delta z = 0.0674\lambda_0$, where $\lambda_0 = 3.11$ GHz. At normal incidence, an electric-field probe was programmed to scan at a constant height of approximately 80% of the height of the object under test. The boxed regions in each panel show where the object under test was placed, and the probe was programmed to scan directly above that region in the indicated area to avoid collisions. In these areas, obviously, the fields appear out of phase compared to the rest of the image, as they refer to a different incidence plane. For oblique incidence, the measurement plane is approximately 50% of the object's height and, in the corresponding panels, the dashed line is below the scan plane and the solid line is above it. The data acquisition system, composed of an Agilent 5071C vector network analyzer (VNA), triggers a Fanuc LR Mate robot arm to make high precision and highly repeatable samples of the electric field in the scan area.

Strong scattering reduction is confirmed by comparing uncloaked and cloaked near-field images. Remarkably, it is seen that for both incident angles the cloak provides excellent cancellation of the scattered fields, as compared to the object alone. In the very near-field, the total fields as measured by the electric-field probe appear almost exactly as the "free space" background measurement in the third column. It should be also stressed that the illuminating Gaussian field pattern contains a more complex angular spectrum than that of the plane wave used in our full-wave simulations, ensuring that the cloak functionality is independent of the illumination form for TM polarization.

Figure 7 shows far-field bistatic RCS measurements along the elevation plane for the cloaked and uncloaked dielectric cylinders; here the scattering gain (in decibels) is specifically defined as the ratio between the RCS of covered and uncovered cylinder, which clearly quantifies the level of scattering suppression by the plasmonic cover. The inset of Figure 7

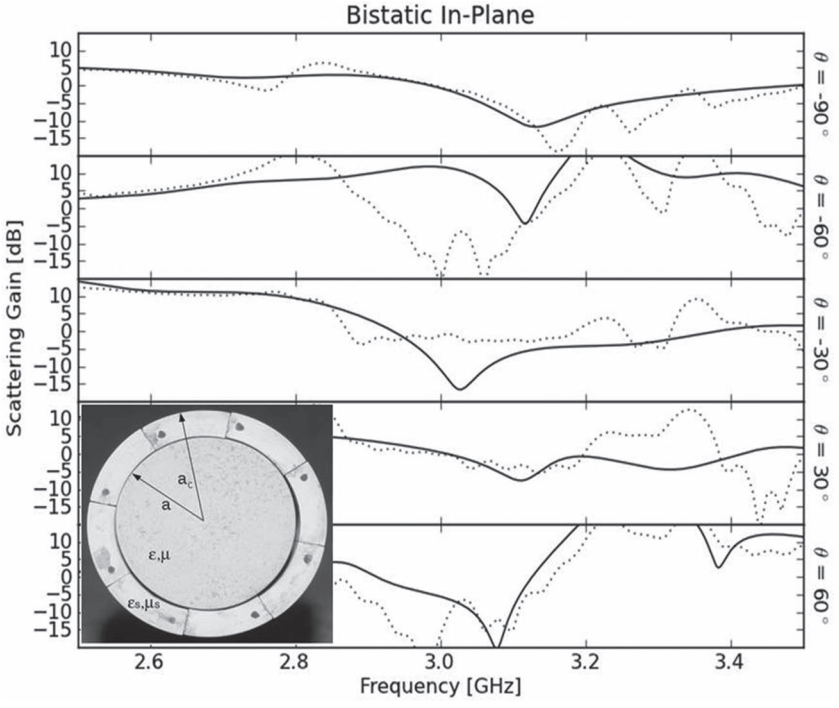

Figure 7. Normalized bistatic measurements along the elevation plane comparing simulation (dotted) and measurement (solid) results. Inset: cross-sectional view with the dielectric target covered by the fabricated cylindrical metamaterial shell. Reproduced with permission.[45] Copyright 2012, Institute of Physics.

© 2012 WILEY-VCH Verlag GmbH & Co. KGaA, Weinheim

15214095, 2012, 44, Downloaded from https://onlinelibrary.wiley.com/doi/10.1002/adma.201202624 by Cochrane Russian Federation, Wiley Online Library on [13/02/2023]. See the Terms and Conditions (https://onlinelibrary.wiley.com/terms-and-conditions) on Wiley Online Library for rules of use; OA articles are governed by the applicable Creative Commons License

15214095, 2012, 44, Downloaded from https://onlinelibrary.wiley.com/doi/10.1002/adma.201202624 by Cochrane Russian Federation, Wiley Online Library on [13/02/2023]. See the Terms and Conditions (https://onlinelibrary.wiley.com/terms-and-conditions) on Wiley Online Library for rules of use; OA articles are governed by the applicable Creative Commons License

shows the cross-section of the real plasmonic cloak, as previously described and characterized.[45] In our measurement, two broadband microwave horns were placed in the far-field of the target ($R = 14\lambda_0 = 140$ cm), where the transmitting antenna was fixed at broadside ($\varphi_{tx} = 0°$, $\theta_{tx} = 90°$), while the receiving antenna was positioned at several elevation angles ($\varphi_{rx} = 0°$, $-90° \leq \theta_{rx} \leq 30°$) to characterize the back- and forward-scattering of the cloaked and uncloaked targets. At each of the viewing angles, relevant RCS suppression is observed around 3.13 GHz. It is remarkably evident here that one may obtain more than 10 dB of suppression of the forward scattering or "shadow" ($\varphi_{rx} = 0°$, $\theta_{rx} = -90°$), which are, in general, the most difficult to suppress. Such a considerable forward scattering reduction further validates the diminishment of the total SCS, consistent with the optical theorem.[79] Here, a slight frequency shift is also observed for increased angles of incidence. As expected, this shift is due to the TM-TE cross polarization coupling for dielectric cylinders.[75,82,83] Based on these near- and far-field scattering measurements, in addition to evidence already previously presented,[45] we have confirmed the robustness and effectiveness of the plasmonic cloak to arbitrary illumination.

4.3. Plasmonic Cloaking at Infrared and Visible Frequencies and Multiband Cloaking

In the previous section, we have shown a plasmonic cloak realized at microwave frequencies using metamaterial technology. Naturally occurring noble metals and doped semiconductors at infrared and visible frequencies can also serve as plasmonic covers to significantly reduce the scattering of nanoparticles and sensors.[19,28–30,34] It is well known that noble metals, such as silver (Ag), copper (Cu), aluminum (Al) and gold (Au), can possess low or negative real permittivity at visible and ultraviolet (UV) frequencies,[6] below the onset of interband transitions. Metals have an abundance of free electrons in the conduction band, providing the negative real permittivity essential for making a plasmonic cloak. Among metals, silver and gold are most popular for plasmonic applications at optical frequencies. Silver has the smallest loss at optical frequencies, while gold has the advantage of being chemically stable in different environments and can be easily deposited as a continuous film. Since aluminum and copper are easily oxidized, their use is usually more challenging for plasmonic applications, in addition to their higher losses.[6]

Recently, it has been reported that some highly-doped wide-bandgap semiconductors, such as gallium zinc oxide (GZO), aluminum zinc oxide (AZO), indium tin oxide (ITO), and titanium nitride (TiN) may display plasmonic properties in the infrared region,[7–10] due to their high carrier mobilities, very high doping levels, and large bandgap and high plasma frequency. All these material characteristics ensure a negative real permittivity and very low interband transition losses at the desired infrared frequencies, which may make them very appealing for plasmonic cloaking in the infrared region. Moreover, we may be able to tailor the plasmonic properties of semiconducting materials with "band engineering", which manipulates and fine tunes the electronic band structure. For instance, the plasma frequency of ITO can be engineered between 0.44 and 6.99 eV by varying the tin (Sn) doping level in In_2O_3 up to 45%.[10] These new plasmonic materials may offer huge potential for realizing plasmonic cloaks in the infrared and telecommunication bands.

However, it remains challenging to find materials whose plasma frequency always coincides with the specific design frequency, and with moderate losses, especially at optical frequencies. As an alternative option, it is possible to extend the previously discussed metamaterial cloak design Figure 3c to the infrared regime.[88] Using plasmonic radial implants in a dielectric shell, we can tune the effective permittivity of the cloak to the desired frequency range. At infrared and optical wavelengths, the finite conductivity and permittivity dispersion of metals should be taken into consideration, which slightly complicate the picture compared to the microwave design.[88] Other implementations of plasmonic cloaking have been demonstrated at ultraviolet and optical frequencies using homogenized metamaterial shells composed of silver nanospheres embedded in a host medium, being either air or silica.[89–92] **Figure 8**a shows a finite-length dielectric cylinder covered by a homogenized cloak, consisting of a periodic arrangement of core–shell nanospheres (silica core covered by silver shell in the silica host medium), as presented elsewhere.[90] The cloak region, designed based on simple Clausius–Mossotti formulas, can exhibit a near-zero effective permittivity at the design frequency 740 THz. Figure 8b,c show the electric field distributions (amplitude and phase) at the design frequency on the central plane orthogonal to the cylinder axis, for Figure 8b,c uncloaked cylinders. It is found that the amplitude and phase of electric fields are largely restored with a properly designed cloak. The robustness of this cloak performance to disorder has also been demonstrated.[90] In addition to the use of plasmonic covers, "anti-phase satellites" have also been successfully proposed for scattering cancellation at IR frequencies, where discrete scatterers, rather than a uniform cover, can be used to strongly reduce the scattering of arbitrarily-shaped objects by destructive interference.[93]

At these frequencies, the physical size of the objects that can be cloaked gets smaller, because of the shortening of the operating wavelength. For this reason, the use of multiple plasmonic layers may be very effective to obtain multiple cloaking frequencies and enlarge the size of the objects to be concealed by cancelling multiple scattering orders.[75] Multi-frequency cloaking methods have been explored by several groups including transformation optics,[94] and Fabry–Perot radial resonances.[95–96] An example of plasmonic multiband cloaking is illustrated in **Figure 9**, where a dielectric nanoparticle with permittivity $\varepsilon = 10\ \varepsilon_0$ and radius $a = 48$ nm is covered by two concentric Drude-like plasmonic shells, with inner radius $a_{in} = 1.25\ a$ and outer radius $a_{out} = 1.15\ a_{in}$, tuned to have negative local polarization at $\lambda_0 = 655$ nm and $\lambda_0 = 480$ nm, respectively, i.e., $\mathrm{Re}\left[\varepsilon_{in}\left(\lambda_0 = 480\ \mathrm{nm}\right)\right] \simeq 0.59\varepsilon_0$, $\mathrm{Re}\left[\varepsilon_{out}\left(\lambda_0 = 480\ \mathrm{nm}\right)\right] \simeq 0.26\varepsilon_0$, $\mathrm{Re}\left[\varepsilon_{in}\left(\lambda_0 = 655\ \mathrm{nm}\right)\right] \simeq 0.23\varepsilon_0$, $\mathrm{Re}\left[\varepsilon_{out}\left(\lambda_0 = 655\ \mathrm{nm}\right)\right] \simeq -0.38\varepsilon_0$. The multiband operation is clearly seen at each design frequency, and in the figure we compare the case of a low-loss Drude profile and of realistic losses. In both scenarios good scattering reduction is observed at both frequencies of operation.

© 2012 WILEY-VCH Verlag GmbH & Co. KGaA, Weinheim

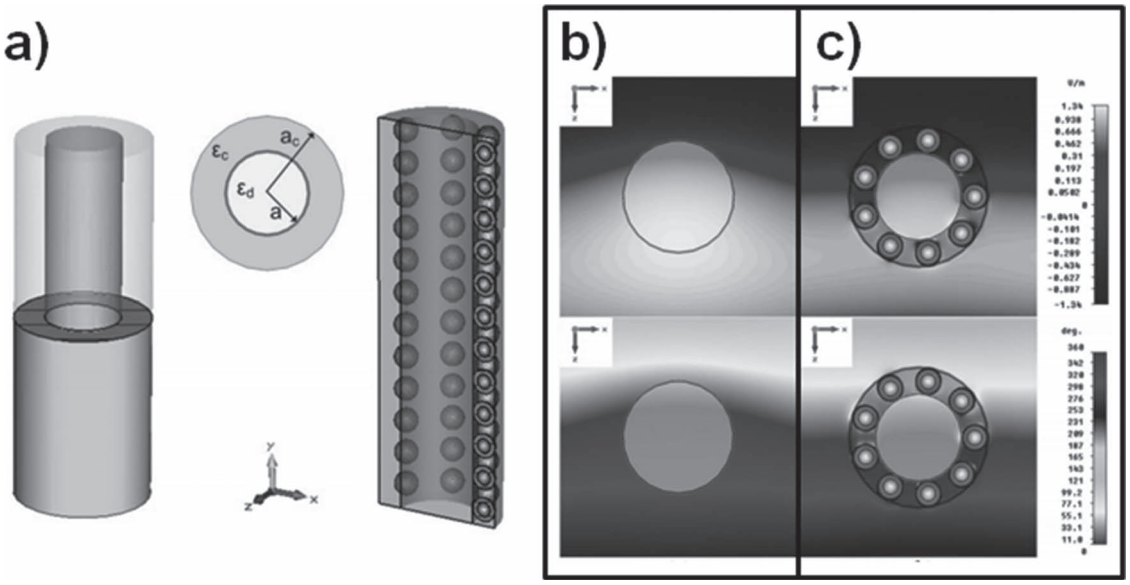

Figure 8. a) Finite-length dielectric cylinder covered by a plasmonic cloak, made of a periodic arrangement of core–shell (silver-silica) nanospheres embedded in the silica host medium. Amplitude (top panel) and phase (bottom panel) of electric fields at the design frequency 740 THz, for a bare (b) and covered (c) dielectric cylinder. Reproduced with permission.[90] Copyright 2011, Optical Society of America.

4.4. Noninvasive Near-Field Sensing Enabled by Plasmonic Cloaking

The scattering and absorption of receiving antennas and sensors is an area of research that spans several decades.[97–104] Antennas and/or sensors that cause minimum scattering, while efficiently receiving the external signal from impinging electromagnetic waves, are generally desired to realize high-quality, low-interference communication and sensing applications. Plasmonic cloaks, or the mantle covers discussed in the next section, may offer an exciting possibility to reduce the structural scattering of receiving antennas and sensors, while efficiently detecting the complex amplitude of electromagnetic waves.[28] Since the field can penetrate into the interior of a plasmonic or mantle cloak, inherent to scattering cancellation techniques, substantial absorption can be induced by an antenna or sensor placed inside the cloak, while its total SCS may be significantly reduced.[28] In principle, it is possible to dramatically reduce the total SCS, leaving only a residual forward scattering signature, or shadow, associated with the power effectively extracted by the sensor.[30]

Cloaked sensors may also have important applications at infrared and optical frequencies, enabling high-performance noninvasive near-field measurements in biological and medical imaging, optical microscopy, nanometer-scale physics, and optical communications by reducing the effect of the measurement apparatus on the measure and restoring the external fields even in the very near-field.[28–30,34] Several recent theoretical and experimental results for "cloaked sensing" applications have appeared in the literature, in which a plasmonic cover was applied to reduce the scattering signature of receiving antennas, semiconductor photodetectors and NSOM tips, making them effectively invisible over a moderately broad frequency range. The idea of suppressing the scattering of a receiving antenna with a plasmonic cloak was originally proposed,[28] and later applied to an aperture NSOM tip in collection mode.[29] The concept was also extended to apertureless NSOM probes by reducing the scattering from the tip walls.[31]

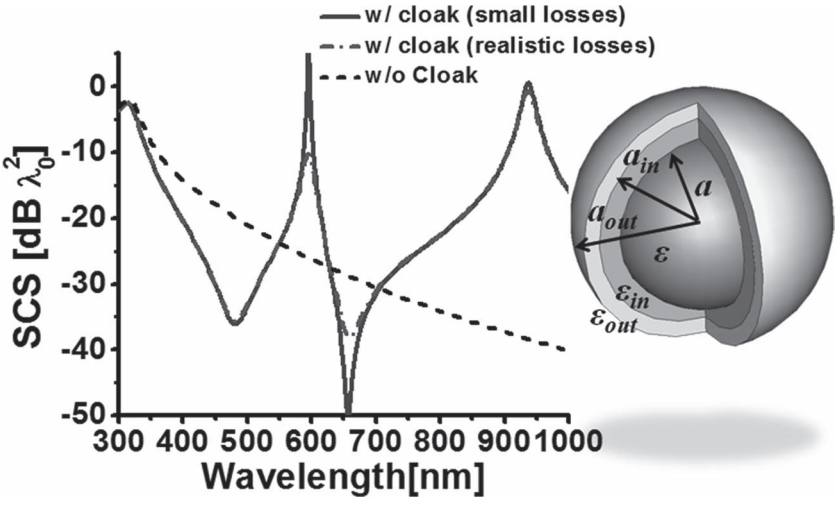

Figure 9. Total scattering cross-section for the two-layer cloak geometry depicted in the inset, for multifrequency operation. Both inner and outer covers follow a Drude model dispersion, considering small ($\gamma = 0.01\omega_p$) and realistic ($\gamma = 0.05\ \omega_p$) Ohmic losses.

© 2012 WILEY-VCH Verlag GmbH & Co. KGaA, Weinheim

15214095, 2012, 44, Downloaded from https://onlinelibrary.wiley.com/doi/10.1002/adma.201202624 by Cochrane Russian Federation, Wiley Online Library on [13/02/2023]. See the Terms and Conditions (https://onlinelibrary.wiley.com/terms-and-conditions) on Wiley Online Library for rules of use; OA articles are governed by the applicable Creative Commons License

15214095, 2012, 44, Downloaded from https://onlinelibrary.wiley.com/doi/10.1002/adma.201202624 by Cochrane Russian Federation, Wiley Online Library on [13/02/2023]. See the Terms and Conditions (https://onlinelibrary.wiley.com/terms-and-conditions) on Wiley Online Library for rules of use; OA articles are governed by the applicable Creative Commons License

This concept was recently experimentally demonstrated at optical frequencies,[34] showing that a plasmonic cover may drastically reduce the scattering of a silicon-nanowire photodetector, while maintaining a good collection of photocurrent. In their experimental setup, gold was deposited on top of a silicon nanowire with a dual functionality: on one hand, it may provide the electrical contact to extract the generated current, at the same time it may operate as a plasmonic cover to suppress its scattering. As mentioned above, at optical frequencies gold may be used as a natural plasmonic material for these purposes. The photodetector was realized by a silicon-nanowire on a gold-coated silica substrate. Excellent optical absorption and photocurrent generation were obtained by the photodetector, supporting the previously discussed idea of "cloaking a sensor." Through a careful design of the gold connectors, the scattered light photodetector has been substantially reduced, while an appreciable photocurrent generation has still been obtained and measured.

4.5. Plasmonic Cloaking for Objects of Arbitrary Geometry

In the previous sections, we have shown the effectiveness of the plasmonic cloaking technique in suppressing the scattering from canonical objects, such as spheres and cylindrical objects.[19,39,45,74] A plasmonic cloak, however, may also be designed for arbitrarily-shaped objects composed of magnetodielectric and conducting materials.[68,84,105,106] In the quasistatic limit, the polarization is dominated by a volumetric effect, whose induced scattering is easily cancelled following the same scheme described above,[19,74] as an integral effect, i.e., by simply tailoring the volume ratio of cloak and object.[106] Even for larger anisotropically-shaped targets, for which the dominant scattering mechanism is generally not only dipolar, total SCS reduction may be obtained by using conformal cloaks with inhomogeneous profiles. With proper designs it is possible to tailor cloaks to successfully reduce the scattering independent of the incident polarization and angle, as discussed in detail elsewhere.[106] In addition, the use of individual anti-phase satellites has also been shown to be very effective for the cloaking of complex and arbitrarily-shaped objects, due to their flexibility in constitutive parameter composition and position about the object.[93]

4.6. Plasmonic Cloaking for Acoustic Waves

In addition to electromagnetic waves over a broad portion of the electromagnetic spectrum, including microwaves, IR and visible frequencies, we have recently applied the plasmonic cloaking technique to acoustic waves with interesting results.[107,108] We have theoretically shown plasmonic cloaking for spheres with different materials, including also the effects of shear waves. Interestingly, we have found that for acoustic waves the plasmonic cloak may be achieved using ordinary fluids and isotropic elastic shells. Although such designs have been shown to be extremely effective, the overall bandwidth is fundamentally limited in this configuration by the flexural shell resonances occurring with isotropic elastic layers. To mitigate these effects, we have also considered spherically isotropic elastic layers, which allow for independent control of the transverse properties, broadening the overall achievable bandwidth. In this context, it is interesting to note that causality issues associated with electromagnetic-wave cloaking are in general more relaxed for acoustic waves, as the propagation velocity in the background medium is much lower. This may allow exciting developments in realizing broadband acoustic scattering suppression.

5. Mantle Cloaking

As an alternative cloaking technique based on scattering cancellation, we have recently proposed to realize *mantle cloaks* based on patterned metallic surfaces.[27] In this case, we cancel the total scattering by inducing suitable surface currents on the cloak surface, which is readily achieved by synthesizing its effective surface impedance with proper patterns. In this case, the surface current induced by the impinging wave radiates "anti-phase" scattered fields that cause destructive interference with the scattered fields produced by the object to be cloaked, thus dramatically reducing the overall visibility of the system. The required surface impedance may be readily realized with metasurfaces and/or frequency-selective surfaces (FSS),[109] with a long history of successful applications in a variety of microwave, millimeter-wave and infrared devices, such as radomes, reflect-array lenses, artificial ground planes, polarizers and filters.[109]

As discussed in the Introduction, metamaterial cloaks are limited by two main factors: bandwidth limitations and the impact of losses and imperfections in the realization of bulk metamaterials. However, mantle cloaks are based on nonresonant features and do not need to rely on metamaterial resonances to induce these effects. For this reason, mantle cloaks may provide good robustness to losses and imperfections.[27] In addition, the low-profile nature of an ultrathin mantle cloak, with negligible thickness may result in improved bandwidth compared to other cloaking techniques.[19,71,110] This simple, low-profile, conformal and light-weight cloaking technique may pave the way for practical cloaking devices, particularly suited for microwave and millimeter-wave or THz technology.

In our first theoretical proposal of a mantle cloak,[27] we assumed that a patterned metallic surface composed of subwavelength periodic structures may be modeled as an isotropic and homogenous averaged surface impedance $Z_s = R_S - iX_S$, relating the averaged tangential electric field at the surface $\mathbf{E}_{tan}$ to the averaged induced surface current $\mathbf{J}_s$ as: $\mathbf{E}_{tan} = Z_s\mathbf{J}_s$, where $\mathbf{J}_s = \hat{\mathbf{r}} \times \left(\mathbf{H}^+_{tan} - \mathbf{H}^-_{tan}\right)$ is induced by the discontinuity of tangential magnetic fields at the surface. This assumption is valid as long as the period of the inclusions is smaller than the wavelength of operation. In this scenario, we have shown theoretically and numerically that a mantle cloak with suitable surface impedance may significantly suppress the scattering from dielectric or conducting objects.[27,111,112]

To analyze the scattering problem we can again use the Lorenz–Mie scattering theory. The expressions of the scattering coefficients for a concentric, spherical object and mantle cloak are given, in a notation consistent with Equation (4), by:[27]

© 2012 WILEY-VCH Verlag GmbH & Co. KGaA, Weinheim

$$U_n^{TM} = \begin{bmatrix} j_n(ka) & j_n(k_0a) & y_n(k_0a) & 0 \\ [kaj_n(ka)]'/\varepsilon & [k_0aj_n(k_0a)]' & [k_0ay_n(k_0a)]' & 0 \\ 0 & \begin{matrix} j_n(k_0a_c)+ \\ +[k_0a_cj_n(k_0a_c)]'/(i\omega\varepsilon_0a_cZ_s) \end{matrix} & \begin{matrix} y_n(k_0a_c)+ \\ +[k_0a_cy_n(k_0a_c)]'/(i\omega\varepsilon_0a_cZ_s) \end{matrix} & j_n(k_0a_c) \\ 0 & [k_0a_cj_n(k_0a_c)]' & [k_0a_cy_n(k_0a_c)]' & [k_0a_cj_n(k_0a_c)]' \end{bmatrix},$$

and

$$V_n^{TM} = \begin{bmatrix} j_n(ka) & j_n(k_0a) & y_n(k_0a) & 0 \\ [kaj_n(ka)]'/\varepsilon & [k_0aj_n(k_0a)]' & [k_0ay_n(k_0a)]' & 0 \\ 0 & \begin{matrix} j_n(k_0a_c)+ \\ +[k_0a_cj_n(k_0a_c)]'/(i\omega\varepsilon_0a_cZ_s) \end{matrix} & \begin{matrix} y_n(k_0a_c)+ \\ +[k_0a_cy_n(k_0a_c)]'/(i\omega\varepsilon_0a_cZ_s) \end{matrix} & y_n(k_0a_c) \\ 0 & [k_0a_cj_n(k_0a_c)]' & [k_0a_cy_n(k_0a_c)]' & [k_0a_cy_n(k_0a_c)]' \end{bmatrix}. \quad (17)$$

Similar to plasmonic cloaks, and consistent with the previous discussions, a dramatic scattering reduction may be achieved by suppressing the U_n coefficients associated with the dominant scattering orders. Conversely, enhanced resonant scattering may be obtained by zeroing the V_n coefficients. For mantle cloaks, both conditions may be achieved with a proper choice of a_c and X_s. In the quasistatic limit, for which ka, $k_0a_c << 1$, the dominant contribution to the scattering is given by the $n = 1$ harmonic, and approximate conditions for cloaking in the two polarizations are obtained in closed form as:[27]

$$TM: \quad X_s = \frac{2\left[2+\varepsilon-\gamma^3(\varepsilon-1)\right]}{3\gamma^3\omega a\varepsilon_0(\varepsilon-1)},$$
$$TE: \quad X_s = \frac{\omega a\mu_0\left[2+\mu+2\gamma^3(\mu-1)\right]}{6\gamma^3(\mu-1)}. \quad (18)$$

When the size of the object is comparable to the wavelength, dynamic formulas (Equation (17)) should be used for the optimal design of a mantle cloak.

Figure 10 shows the variation of the total SCS with surface reactance for an ideal mantle cloak, placed directly on the surface of a dielectric sphere with permittivity $\varepsilon = 10\ \varepsilon_0$ and diameter d = 2a for different frequencies of operation. For a fair comparison, the case of a bare dielectric sphere (dashed line) is also presented. With optimal surface reactance values, all mantle cloaks in Figure 10 display over 90% reduction in the total SCS. For different surface reactance values, resonant scattering peaks are also obtained, corresponding to the dual condition $V_n = 0$, for various values of n and TE or TM scattering coefficients. Figure 10 shows how the optimal value of surface reactance varies with the geometry, material and size of the object to be cloaked. Typically, the surface reactance X_s may assume a wide range of values, as a function of the metasurface geometry and the operating frequency. It has been demonstrated that a suitably designed mantle cloak can achieve significant scattering reduction over a moderately broad range of frequencies, without the need of bulk metamaterials.[27,112–114]

As observed by tracking the minima in Figure 10 or looking at Equation (17), the required surface reactance has a negative dispersion with frequency, implying that very broadband cloaking may not be achieved with any passive metasurface, as it is bounded to satisfy the Foster's reactance theorem. According to this theorem,[115] the reactance of any passive system or network with small losses should monotonically increase with frequency. This is evidence of a general limitation of any passive cloaking technique, for which the bandwidth is always fundamentally limited by causality and passivity, and it decreases with the overall size of the object to be cloaked. Compared to other cloaking techniques, however, mantle cloaking provides a comparatively larger bandwidth of operation. In addition, we are currently exploring the possibility to realize *active* metasurfaces by loading patterned conducting surfaces with active circuits,

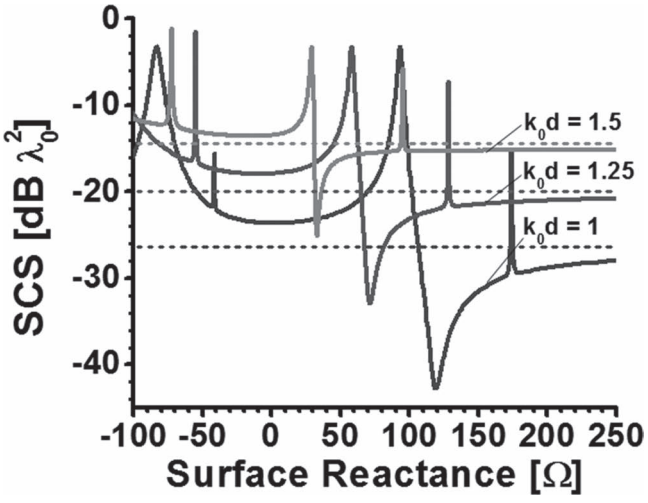

Figure 10. Variation of the total SCS versus surface reactance for a cloaked dielectric sphere with permittivity $\varepsilon = 10\ \varepsilon_0$; different electrical size k_0d are considered.

© 2012 WILEY-VCH Verlag GmbH & Co. KGaA, Weinheim

15214095, 2012, 44, Downloaded from https://onlinelibrary.wiley.com/doi/10.1002/adma.201202624 by Cochrane Russian Federation, Wiley Online Library on [13/02/2023]. See the Terms and Conditions (https://onlinelibrary.wiley.com/terms-and-conditions) on Wiley Online Library for rules of use; OA articles are governed by the applicable Creative Commons License

ADVANCED OPTICAL MATERIALS
www.advopticalmat.de

15214095, 2012, 44, Downloaded from https://onlinelibrary.wiley.com/doi/10.1002/adma.201202624 by Cochrane Russian Federation, Wiley Online Library on [13/02/2023]. See the Terms and Conditions (https://onlinelibrary.wiley.com/terms-and-conditions) on Wiley Online Library for rules of use; OA articles are governed by the applicable Creative Commons License

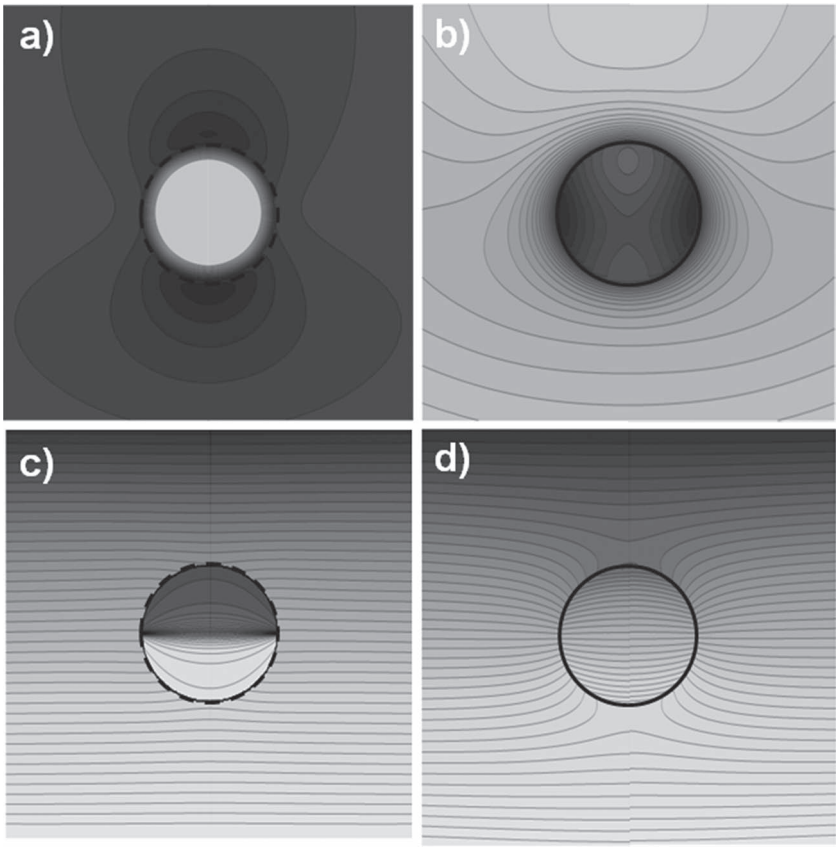

Figure 11. Amplitude of the electric field on the H plane for a dielectric sphere with $\varepsilon = 10$ and $k_0 d = 1.25$, (a) with and (b) without a conformal mantle cloak. (c) and (d) are similar to (a) and (b), but for the phase of the magnetic field on the E plane.

such as negative impedance converters (NICs) or non-Foster lumped elements, to overcome Foster's theorem limitations. This may allow breaking the limit on "positive-slope" reactance dispersion and enhance the bandwidth of operation, which has recently become an active research topic in the metamaterial society for other types of applications.[116–117]

Figure 11 shows the amplitude of the electric field on the H plane for a dielectric sphere with permittivity $\varepsilon = 10\ \varepsilon_0$ and electrical size $k_0 d = 1.25$, with Figure 11a and without Figure 11b a conformal passive mantle cloak, designed to have the required surface reactance $X_s = 71.3\ \Omega$ at the design frequency. Plane-wave illumination is considered from the bottom and different panels in Figure 11 are plotted in the same color scale for fair comparison. Figure 11c,d show similar plots for the phase of the magnetic field on the E plane. It is seen that a mantle cloak with suitable surface reactance may largely reduce the scattering and restore unperturbed planar wavefronts around the cloak, even in the very-near field. We note that, unlike transformation-based cloaks that completely isolate their interior, the field penetration inside the sphere covered by plasmonic or mantle cloaks may allow the detection of impinging signals by an observer or sensor placed inside the cloak. This is of interest for emerging applications in cloaked sensing, noninvasive probing, and low-interference communication.[28]

A similar design recipe, considered in **Figure 12**, can be used for effectively cloaking a conducting sphere covered by a mantle cloak. In this case, a gap between the shunt impedance of the mantle cloak and the conductor is necessary to avoid an electric short. Here we choose the radius of mantle cloak 1.2 times larger than the conducting sphere. Figure 12 shows the total SCS versus the surface reactance for different electrical sizes of conducting spheres. It is evident that, with optimal surface reactances, we may obtain remarkable scattering reductions for all the considered cases. The achievable scattering reduction for conducting objects is lower than the one for dielectric objects, due to larger contributions from additional multipole scattering orders and the impenetrability of the object. In this context, it is worth mentioning that in order to make a cloak design independent of the object to be hidden, as it is the case for the other cloaking techniques discussed in Sections 3 and 4, we may consider coating the cloak with an impenetrable surface, such as a perfect conductor. If the object to be hidden is, however, penetrable, this has two major disadvantages: by requiring internal isolation and rerouting of the impinging energy around the cloak we necessarily reduce the overall bandwidth of operation and we additionally isolate the cloak interior, not ideal in case we want to observe or sense the outside. As an aside, implicitly this is what happens when choosing the transformation-based cloaking approach.

Figure 13 shows the amplitude of the electric field on the H plane for a conducting sphere with electrical size $k_0 d$ =1.25, illuminated by a plane wave from the bottom, with Figure 13a and without Figure 13b the mantle cloak in Figure 8. Figure 13c,d show the phase distribution of the magnetic field on the E plane.

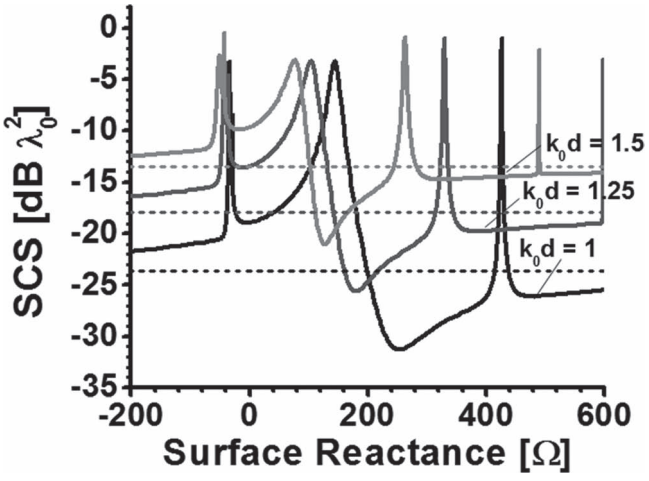

Figure 12. Variation of the total SCS versus surface reactance for a cloaked conducting sphere with different electric size.

© 2012 WILEY-VCH Verlag GmbH & Co. KGaA, Weinheim

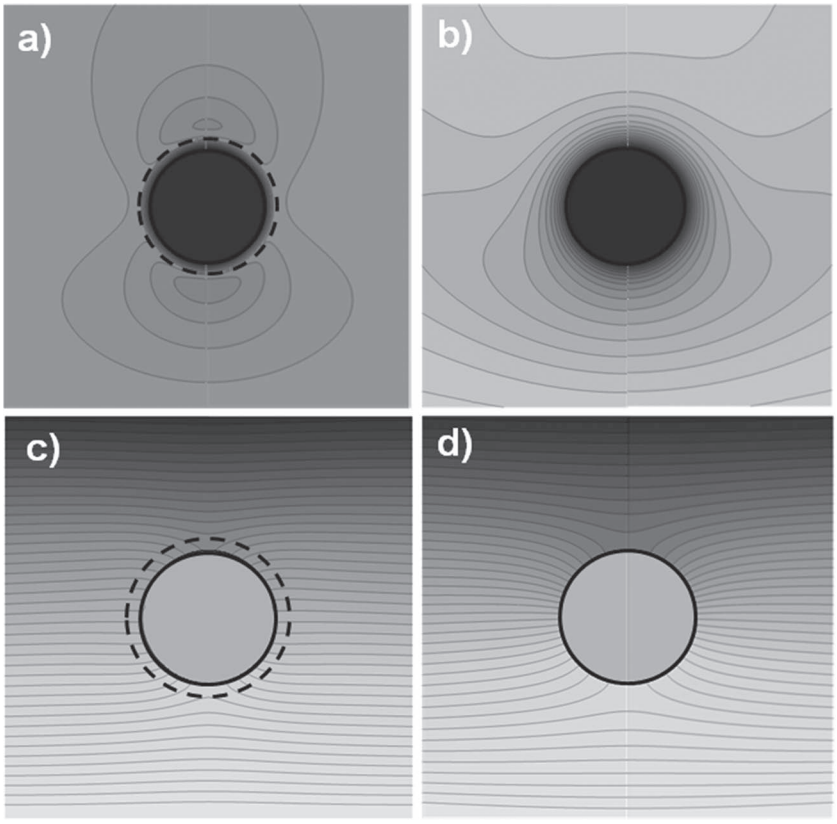

Figure 13. Amplitude of the electric field on the H plane for a conducting sphere with k_0d = 1.25, (a) with and (b) without a mantle cloak with radius 1.2 times larger than the object. (c) and (d) are similar to (a) and (b), but for the phase of the magnetic field on the E plane.

Similar features on the restoration of uniform amplitude and planar phase fronts are verified also in this 3D conducting geometry, even though the cloaked object here is impenetrable. Similar considerations may be applied to cylindrical shapes, as discussed in the previous section for the plasmonic cloaking, as well as for arbitrary configurations. Here we should specifically note that a 2D mantle cloak with a capacitive patterned surface may provide large scattering reduction for elongated conducting objects,[111,112] showing a much lower visibility compared to the previously discussed plasmonic cloaks. This is mainly due to the more efficient cancellation of the dominant scattering coefficient c_0^{TM},[111,112] which is hardly cancelled by the plasmonic cloak in the quasistatic limit [see Equation (14)]. In the following, we discuss practical designs and recipes to realize mantle cloaks in different frequency regimes, ranging from RF to THz and near-infrared frequencies. Although their realization and synthesis will strongly depend on the frequency range in terms of available materials, the same physical principle may be applied, providing similar performance for comparable electrical sizes, consistent with the theoretical results presented in this section.

5.1. Mantle Cloak Realization at Radio and Microwaves Frequencies

Frequency selective surfaces and metasurfaces have been extensively studied at RF for filtering and antenna applications, and a large body of literature is available on different geometries and structures to realize the desired surface reactance at these frequencies. Metals behave almost as perfect conductors at microwaves, allowing the synthesis of almost lossless reactive surfaces. Various surface structures have explicit analytical design formulas (i.e., grids, strips, cross dipoles, and Jerusalem crosses) which we have recently successfully applied to the design of conformal mantle cloaks for cylindrical dielectric and conducting objects.[109,118–120] Also, more sophisticated patterns have been explored, whose design requires numerical simulations and optimization procedures to broaden the bandwidth of operation and enhance their performance.[121,122]

For objects with transverse sizes comparable to the wavelength, this technique has shown to be very effective in suppressing the total SCS. For instance, we have recently proposed a practical implementation of an RF cloak made of a simple conducting helical sheath, whose surface impedance, although being anisotropic, can still provide scattering cancellation for dielectric cylinders over a moderately broad bandwidth.[113] This simple conducting sheath possesses an inductive nature, similar to a simple winding wire that can compensate the capacitive fields around a thin dielectric rod. Our numerical results show that, by properly choosing the pitch angle of the conducting helix, the TM scattering from a dielectric cylinder may be drastically suppressed over a moderately broad bandwidth.[113] However, TE scattering, which is less relevant for moderately sized elongated dielectric objects, is not suppressed by this helical structure, and therefore alternative FSS designs, arguably more complex, should be considered. We should also highlight that the anisotropic surface impedance of a conducting helical sheath may deteriorate the cloaking performance, due to inherent cross-polarization coupling even for normal incidence, analogous to the previously discussed oblique incidence for 2D plasmonic cloaks. In order to realize high-performance mantle cloaks, it is relevant to design surface structures that realize homogenous and possibly isotropic surface impedances, in order to eliminate cross-polarization coupling and residual scattering. In this regard, we have proposed interesting mantle cloaking geometries for cylindrical and spherical geometries, some of them possessing a large degree of isotropy.[111,112,118–120]

The inset of **Figure 14** shows a design example of a practical mantle cloak: a 3D dielectric sphere with diameter $2a = \lambda_0/4$ and permittivity $\varepsilon = 10\ \varepsilon_0$ is covered by a mantle cloak with radius $a_c = 1.1a$. Figure 14 shows the SCS versus frequency for this object with and without cloaking, showing that for a TM-polarized plane wave, this anisotropic mantle cloak may considerably reduce the scattering and the overall visibility at the design frequency. The inset of Figure 14 shows the far-field scattering patterns for the dielectric sphere with and without

© 2012 WILEY-VCH Verlag GmbH & Co. KGaA, Weinheim

15214095, 2012, 44, Downloaded from https://onlinelibrary.wiley.com/doi/10.1002/adma.201202624 by Cochrane Russian Federation, Wiley Online Library on [13/02/2023]. See the Terms and Conditions (https://onlinelibrary.wiley.com/terms-and-conditions) on Wiley Online Library for rules of use; OA articles are governed by the applicable Creative Commons License

15214095, 2012, 44, Downloaded from https://onlinelibrary.wiley.com/doi/10.1002/adma.201202624 by Cochrane Russian Federation, Wiley Online Library on [13/02/2023]. See the Terms and Conditions (https://onlinelibrary.wiley.com/terms-and-conditions) on Wiley Online Library for rules of use; OA articles are governed by the applicable Creative Commons License

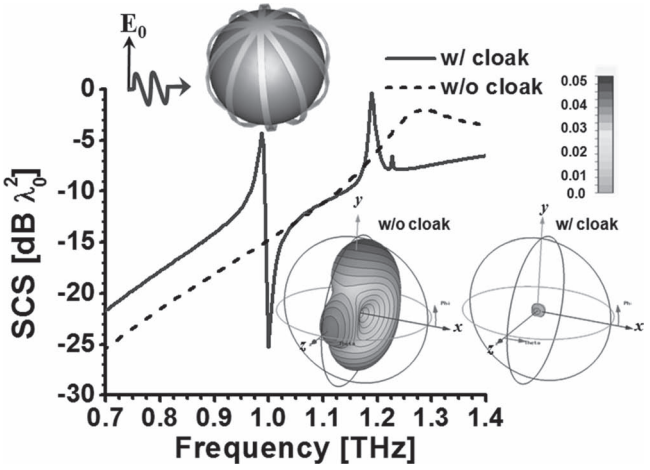

Figure 14. Practical mantle cloak design for a dielectric sphere with diameter $2a = \lambda_0/4$ and $\varepsilon = 10\ \varepsilon_0$ and total SCS variation with frequency. The far-field scattering patterns for this dielectric object with and without the coverage of the mantle cloak are shown in the insets.

the mantle cloak, further confirming that the scattering can be largely suppressed at all angles.

5.2. Mantle Cloak Realization at Terahertz and Infrared Frequencies

There is growing interest in graphene-based technology, and in this section we discuss how this *one-atom-thick* nanomaterial, with dynamically tunable electromagnetic properties, may serve as a building block to realize tunable and switchable far-infrared (FIR) and THz mantle cloaks. *Real-time* tunability may represent an exciting property for THz cloaks and graphene may provide tremendous advantages in this sense compared to any other natural material. Graphene possesses a truly 2D electronic system composed of a one-atom-thick planar sheet of sp^2-bonded carbon atoms arranged in a hexagonal lattice.[12] A graphene monolayer may be described as a gapless semiconductor, with massless and linear long-wavelength Dirac dispersion and Fermi velocity $v_F = 10^8$ cm/s.[12] Clean and chemically doped graphene is particularly interesting for its relatively low-loss surface reactance at infrared frequencies (until the threshold of interband transition $2|\mu_c| = \hbar\omega$, where μ_c is the Fermi energy or chemical potential of graphene), ideal to tailor the surface current at will. For realistic carrier densities of graphene in the range 10^{11}–10^{13}cm^{-2}, the interband threshold can be continuously tuned up to near-infrared frequencies. Its large conductivity and tunability, which dynamically respond to an applied bias voltage, may provide exciting venues to achieve scattering cancellation, as we recently proposed.[114] The progress in synthesizing large-area graphene by chemical vapor deposition (CVD),[121–123] in addition, may provide more in general a promising route towards realizing graphene-based devices like this one. In this regard, graphene's excellent electronic and optical properties, as well as its high thermal conductivity and mechanical strength, combined with its extreme thinness (≈3.3 Å),[12] have raised remarkable interest in high-speed electronics (i.e., graphene-based field-effect transistors) and photonic devices (i.e., THz oscillators and low-noise sensors).[124–126] More interestingly, recent theoretical and experimental works have shown how a graphene monolayer can support the intraband plasmon excitation and surface-plasmon polariton waves in the THz and far-infrared spectrum, with relatively low loss, strong wave localization, and long plasmon propagation.[127–131] These peculiar properties of graphene have been recently suggested to realize transformation metamaterials and flatland optics on a one atom-thick surface in the infrared spectrum.[128]

We can describe the graphene layer with a complex-valued surface conductivity $\sigma_s(\omega) = \sigma'_s - i\sigma''_s$ that is dependent on the applied chemical potential μ_c (or Fermi energy), which can be tuned either *passively*, by tailoring the doping profile (density and type of carriers) or by chemical surface modification (i.e., carboxylation and thiolation).[129–135] Furthermore, *active* tunability is made possible by applying either an external static electric field (resulting in an isotropic scalar surface conductivity), or an external static magnetic field via Hall effects (resulting in anisotropic and tensor surface conductivity).[129–133] Graphene's surface conductivity may be modeled using the well-known Kubo formula.[129–133] In the THz and FIR regions, below the interband threshold and the optical phonon frequency ($\hbar$ is the reduced Planck's constant),[129–133] only the intraband contribution dominates and the direct interband electron transition is usually negligible. The unique features of ballistic transport and ultrahigh electron mobility (in excess of 20 000 cm^2 V^{-1} s^{-1}) provides graphene with an overall low-loss atomic-scale conduction surface.[125] The intraband electron-phonon scattering process, mainly depending on impurities and defects, can be explicitly written as

$$\sigma_{\text{intra}} = \mathrm{i}\frac{\mathrm{e}^2 \mathrm{K_B T}}{\pi\hbar^2\,(\omega + \mathrm{i}\,\tau^{-1})}\left[\frac{\mu_c}{\mathrm{K_B T}} + 2\ln\left(\exp\left(-\frac{\mu_c}{\mathrm{K_B T}}\right)+1\right)\right], \quad (19)$$

where e is the electron charge, K_B is the Boltzmann constant.[133] The momentum relaxation time τ (inverse of the electron-phonon scattering rate), due to carrier intraband scattering, accounts for plasmon losses that depend on impurities and defects. Here we assume a temperature T = 300 K and $\tau = 0.5$ ps, which is consistent with ballistic transport features of graphene, and whose mean free path was measured to be up to 500 nm at room temperature and larger than 4 μm at lower temperatures.[136] $|\mu_c| >> K_BT$, Equation (19) reduces to the Drude-like expression

$$\sigma_{\text{intra}} \simeq \frac{e^2\mu_c}{\pi\hbar^2}\frac{i}{(\omega + i\,\tau^{-1})}. \quad (20)$$

The unique features of ballistic transport, ultrahigh electron mobility and electron (hole) concentrations as high as $n_e \approx 10^{13}$ cm^{-2} may provide an excellent figure of merit FOM = $|\sigma''_s/\sigma'_s|$ in the frequency range of interest. Therefore, clean graphene with low defect and impurity levels may effectively make a low-loss inductive atomic surface at THz and FIR, playing the same role as the low-loss reactive FSS at RF considered in the previous section, but without the fabrication challenge of patterning microstructured, homogeneous and isotropic surfaces over an atom-thick layer.

© 2012 WILEY-VCH Verlag GmbH & Co. KGaA, Weinheim

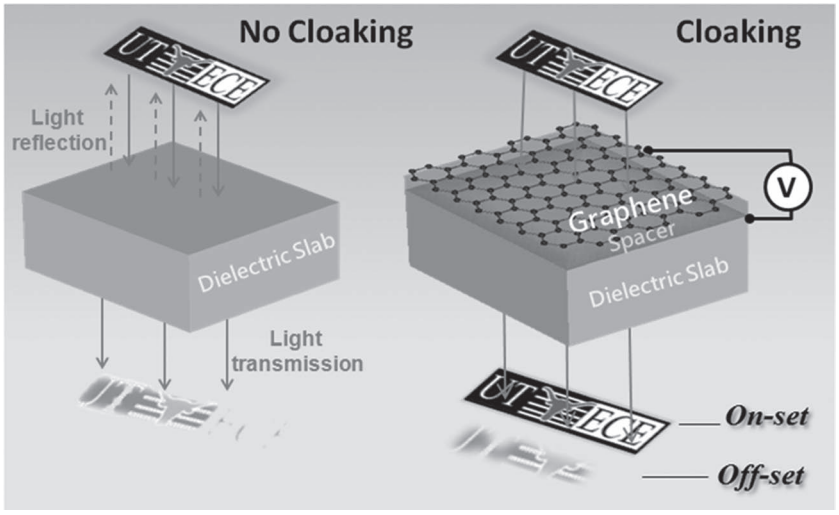

Figure 15. Schematic diagram of a planar mantle cloak realized with a graphene surface cloak: an atomically thin graphene monolayer grown on spacer (i.e., SiO_2) to cloak a dielectric planar slab. We notice that, with a bottom-gate structure (see schematics on the right), the surface conductivity of graphene, as well as the overall cloaking effect, may be dynamically tuned and switched.

We have shown the potential of realizing a mantle cloak using a graphene monolayer:[114] **Figure 15** shows a simple one-dimensional (1D) scenario, in which a graphene surface cloak (left panel), formed by a graphene monolayer with suitable chemical potential, is used to suppress the reflections from a dielectric substrate. The graphene cloak is supported by a thin-film spacer (i.e., silicon dioxide (SiO_2)) and is placed on top of a dielectric slab, which we intend to cloak and make transparent at the design frequency. By using a simple transmission line model to approach this 1D boundary-value problem,[114] it is possible to show that the proper choice of surface reactance can make the input admittance at a given distance from the dielectric slab equal to the background line admittance, completely suppressing the reflected wave at the frequency of interest. This transparency effect is based on scattering cancellation and holds independent of the total thickness of the structure, which is different from a conventional Fabry–Perot resonant tunneling. Due to the 1D geometry considered here, this is effective only as long as the object to be cloaked is penetrable and low-loss. We should stress that this graphene-induced transparency is very distinct from planar carpet cloaks, which are designed to cancel the back reflections from a bump on a planar mirror, rather than to make the whole substrate transparent.

More interestingly, the functionality of this graphene cloak may be tuned by adjusting the chemical potential that is modified by the induced carrier density. This implies that a polysilicon gate realized behind the SiO_2 layer may be able to tune and switch the cloaking operation, envisioning an ultrathin, dynamically tunable infrared mantle cloak comprised of graphene and integrated circuitry. Typically, the chemical potential may be tuned up to ≈1–2 eV by standard values of an externally applied bias.[11,12] As illustrated in **Figure 16**, the scattering at the operating frequency may be switched from "cloaked" to "uncloaked" states, by simply changing the graphene chemical potential.[114] Such "ON" and "OFF" response is very promising to realize *active* tunable cloaks as well as IR switching and modulating devices, with a voltage-controlled and electrically-driven transmission.

This concept can be extended to a 2D geometry by envisioning the use of a graphene microtube (or single-walled metallic carbon microtubes with the same energy dispersion).[136–139] like in the case of a dielectric cylinder wrapped by a graphene monolayer. We consider an impinging TM polarized plane wave at different angles of incidence α, as illustrated in Figure 16a, which is the case of most interest for scattering reduction purposes in this scenario. Figure 16b shows the total SW for an infinite core–shell dielectric cylinder with a core diameter $2a = \lambda_0/5$ and permittivity $\varepsilon = 5\varepsilon_0$ surrounded by a SiO_2 shell with radius $a_c = a$ and permittivity $\varepsilon = 3.9\varepsilon_0$. This core–shell cylinder is covered by a graphene-wrapped microtube with optimal chemical potential μ_c = 0.606 eV and momentum relaxation time (effectively the loss factor) varied from τ = 1 ps to τ = 0.1 ps. The figure shows how a graphene cloak may realize significant scattering suppression at the design frequency f_0 = 2 THz, even after considering realistic loss on the graphene surface. The cloaking performance is quite robust to absorption, even for short relaxation times corresponding to high intrinsic losses. Figure 16c shows the scattering gain, defined as the ratio of total SW between the cloaked and uncloaked cylinders, for different angles of incidence; here the momentum relaxation time of graphene is fixed to 0.5 ps. It is evident that this graphene cloak can efficiently suppress the scattering (negative gain in dB in the figure) at the design frequency, for a broad range angles of incidence between 30° and 90°. This is conceptually similar to cylindrical plasmonic cloaks even if it is now obtained with a single atomic layer.[45,74] From the material point of view, we notice that, even when we consider a regular periodic array of small inclusions, like in the RF mantle cloaks considered in the previous sections, we obtain a surface impedance that is in general a function of the incident angle in cylindrical geometries, due to inherent spatial dispersion effects.[118–120] However, a graphene monolayer composed of compactly arranged carbon atoms (which is "extremely" deep-subwavelength), can be considered an ideal homogeneous, isotropic surface at THz, with a surface conductivity independent of the incident angle and polarization. This not only simplifies the design, but it also allows realizing mantle cloaks with robust angular performance.

Figure 16d shows the SW as a function of frequency for the cloaked cylinder. Here we specifically vary the graphene's chemical potentials from 0.3 to 0.8 eV. The cloaking frequency may be significantly tuned by changing the chemical potential, showing great possibilities to realize a tunable and switchable cloaking device. At specific frequencies, it is possible to vary the total scattering width by over two orders of magnitude by simply

© 2012 WILEY-VCH Verlag GmbH & Co. KGaA, Weinheim

15214095, 2012, 44, Downloaded from https://onlinelibrary.wiley.com/doi/10.1002/adma.201202624 by Cochrane Russian Federation, Wiley Online Library on [13/02/2023]. See the Terms and Conditions (https://onlinelibrary.wiley.com/terms-and-conditions) on Wiley Online Library for rules of use; OA articles are governed by the applicable Creative Commons License

15214095, 2012, 44, Downloaded from https://onlinelibrary.wiley.com/doi/10.1002/adma.201202624 by Cochrane Russian Federation, Wiley Online Library on [13/02/2023]. See the Terms and Conditions (https://onlinelibrary.wiley.com/terms-and-conditions) on Wiley Online Library for rules of use; OA articles are governed by the applicable Creative Commons License

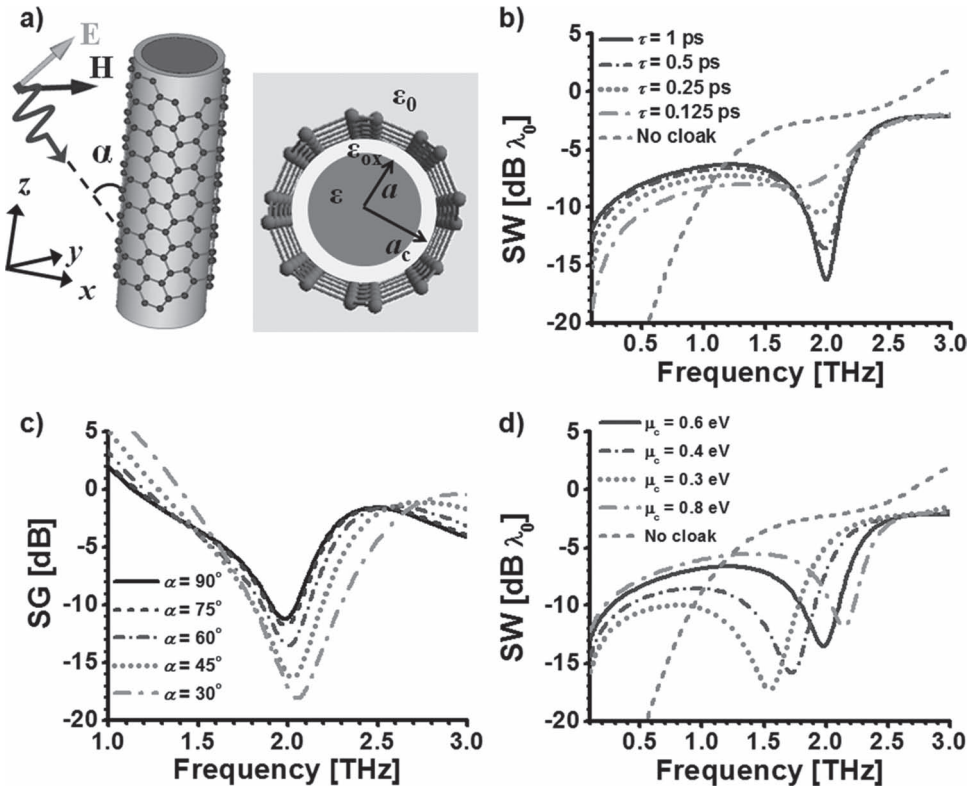

Figure 16. a) THz mantle cloak made of a graphene-wrapped microtube with $\mu_c = 0.606$ eV and $\tau = 0.5 \times 10^{-12}$ s, designed for an infinite core–shell dielectric cylinder with core diameter $2a = \lambda_0/5$ and permittivity $\varepsilon = 5\ \varepsilon_0$, surrounded by a SiO_2 shell with radius $a_c = 1.1a$ and permittivity $\varepsilon = 3.9\varepsilon_0$. b) Total SW of the core–shell cylinder with and without cloak, varying the momentum relaxation time τ. (c) is similar to (b), but showing the scattering gain for different incidence angles. (d) is similar to (b), but for different chemical potentials of graphene.

varying the graphene's chemical potential. Finally, we note that in the THz and infrared regimes these graphene-based metasurfaces have very exciting properties in terms of loss levels and large tunability, beyond the cloaking application.[140] In the future, we envision that graphene may provide a wide range of possibilities in a variety of THz applications, such as tunable, switchable, and electrically-programmable devices, amplitude and phase modulators, biomedical sensors and detectors, imaging, communication components, and devices to control radiation and absorption.

5.3. Realization of Mantle Cloaks at IR and Visible Frequencies

For operating frequencies larger than tens of THz, patterning micro-/nanodimensional FSS and metasurfaces on curved substrates is quite challenging, as the periods required to realize a fairly homogeneous surface reactance are in the order of few nanometers. At these larger frequencies, moreover, graphene's surface conductivity does not provide the same exciting properties as in the THz range, due to the interband transition loss and optical phonon scattering (while acoustic phonon scattering is dominant at longer wavelengths), and it becomes practically constant, equal to $e^2/4\hbar$.[127] To extend the concept of mantle cloaking in this frequency range, new solutions and/or novel materials should be considered.

We can achieve this by applying the concepts of optical nanocircuit theory,[140,141] which allows translating the conventional circuit concepts to optical frequencies, based on displacement rather than conduction effects. This effectively allows realizing inductive or capacitive surfaces using materials with negative or positive real permittivity, respectively. Since mantle cloaking relies on an ultrathin reactive surface, we may expect that a patterned nanocircuit layer, with controllable inductive or capacitive properties, may be able to tailor the surface current at short wavelengths, infrared and even optical frequencies, effectively realizing the principle of mantle cloaking. **Figure 17**a shows the schematics of a near-IR mantle cloak made of a silver ultrathin film, with gaps filled by dielectrics (i.e., capacitive loads), which may enable tuning the cloak operating frequency as a nano-*LC* filtering surface,[142,143] as schematically depicted in Figure 17b. In this nanocircuit model, the applied source corresponds to the impressed optical field, L_c and R_c are the inductance and resistance (due to material absorption) of the metallic layer, C_c and C_s are the capacitances associated with the load at the gap and the dielectric object, and C_f is the one related to the fringing fields around the particle.[140–143] Nanocircuit theory allows tailoring the surface reactance of the cloak to achieve the required value that cancels the scattering from the object.

Consider first an unloaded silver film, similar to the plasmonic cloaking scenario discussed in the previous section. Under the assumption that the silver thickness Δ is

© 2012 WILEY-VCH Verlag GmbH & Co. KGaA, Weinheim

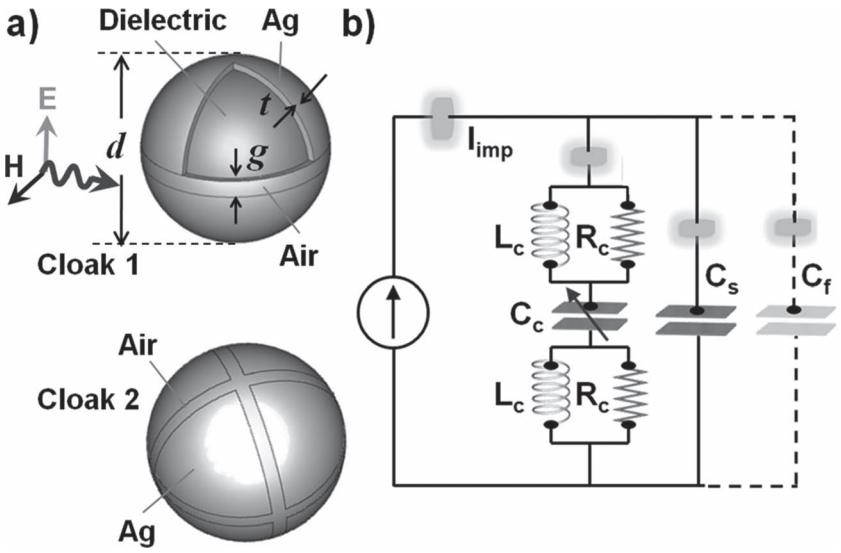

Figure 17. a) Schematic of a nanocircuit-inspired mantle cloak in the near IR. b) Nanocircuit model for cloak 1 in (a).

small, we can describe its equivalent surface conductivity as $\sigma_s = -i\omega\Delta\left(\varepsilon_{Ag}(\omega) - \varepsilon_0\right) = \omega\Delta \mathrm{Im}[\varepsilon_{Ag}] + i\omega\Delta(\varepsilon_0 - \mathrm{Re}[\varepsilon_{Ag}])$, where ε_{Ag} is the silver permittivity, following a Drude-type dispersion.[144] If we would like to cloak a dielectric object with permittivity $\varepsilon = 10\ \varepsilon_0$ and diameter $2a = 600$ nm at the operating frequency $f_0 = 110$ THz, the required surface reactance $X_s = 42.45\ \Omega$. Applying the nanocircuit concept, this value can be achieved with a 10-nm-thick silver nanofilm, realizing an effective surface impedance $X_s = 1.69 - i42.25\ \Omega$. **Figure 18**a shows the calculated SCS versus frequency for four different scenarios: (i) a dielectric spherical object with permittivity $\varepsilon = 10\ \varepsilon_0$ and diameter $2a = 600$ nm (gray dashed line), (ii) a silver sphere with same size (black dash-dot), (iii) a dielectric sphere covered with a 10-nm-thick silver thin film, and (iv) a dielectric sphere covered with a 6-nm-thick silver, providing an effective surface impedance $X_s = 2.8 - i\ 63.9\ \Omega$. We see how an ultrathin silver layer can drastically reduce the total SCS around the design frequency compared to the pure dielectric or silver spheres. Moreover, by changing the thickness and the corresponding effective surface reactance, the SCS dip and cloak's operating frequency can be tuned to a large degre

It is interesting to note that this design could also have been synthesized using the plasmonic cloaking approach described above. The nanocircuit cloak allows connecting the plasmonic and mantle cloaking techniques and extending them to different scenarios and possibilities. In fact, we may now tune the cloaking frequency and scattering properties by loading the designed mantle cloak with lumped nanocircuit elements, as schematically considered in Figure 17a. Figure 18b shows the total SCS versus frequency, based on full-wave simulations,[86] for five different scenarios: (i) a dielectric spherical object with permittivity $\varepsilon = 10\ \varepsilon_0$ and diameter $2a = 832$ nm (gray dashed line), (ii) a silver sphere with same size (black dash-dot), (iii) a dielectric sphere covered with cloak 1 in Figure 17a, with a gap height $g = 100$ nm and thickness of silver layer $t = 33.3$ nm (in this configuration, we assume an air gap), (iv) a similar configuration, but loading the gap with GaAs ($\varepsilon = 12.5\ \varepsilon_0$), (v) a dielectric sphere covered with cloak 2, with air gaps, $g = 100$ nm and $t = 33.3$ nm. The last design is quasi-isotropic and less polarization sensitive. In this case, the gaps in the silver film allow adding a nanocapacitance in the nanocircuit model for the cloak, and control its functionality as a nanofilter element.[145] As seen in Figure 18b, suitable cloak designs following this approach may significantly reduce the total SCS at the design frequency, as a function of the number of gaps and loading materials, as predicted from optical nanocircuit theory. Here we specifically highlight the design flexibility of these nanocircuit-inspired mantle cloaks. For instance, even though the uncloaked objects have different physical sizes in Figure 18a,b, we may achieve comparable cloaking performance at the same frequency by properly selecting lumped nanocircuit elements, tailoring the effective surface reactance.

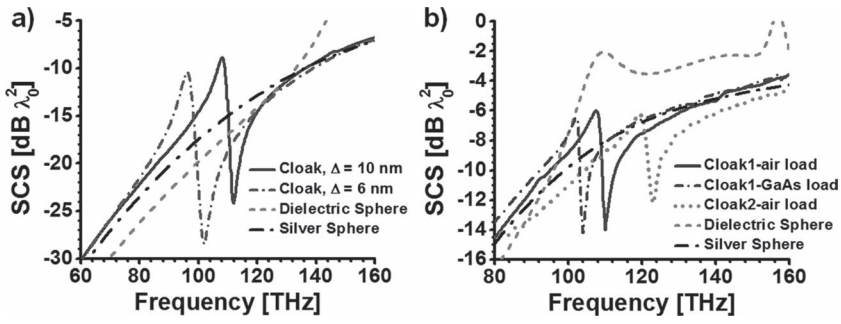

Figure 18. a) Variation of the total SCS versus frequency for a dielectric sphere with $\varepsilon = 10\varepsilon_0$ and $2a = 600$ nm, covered by a silver film with thickness of 6 nm (dash-dot-dash) and 10 nm (solid). (b) is similar to (a), but for a larger dielectric sphere with $2a = 832$ nm covered with different nanocircuit-based mantle cloaks shown in Figure 17. In both panels, the dielectric (grey dash) and silver sphere cases (black dash-dot) are also shown for comparison.

Figure 19a,b show the distribution of electric field amplitude on the E-plane for a dielectric sphere covered by cloak 1 and cloak 2, respectively, at the design frequency; here we assume an air gap for both cases. For fair comparison, the uncloaked sphere is also shown in the same scale. We clearly see how most of the plane wave impinging on the cloaked sphere can pass through the cloaked object without much perturbation. This is simply obtained by using an ultrathin silver film with capacitive slots, without the need of bulky metamaterial or plasmonic materials. This cloaking effect may also be self-tuned, for instance considering nonlinear effects in the cloak with strong third-order Kerr nonlinearities, similar to our previous nonlinear nanoantenna and nonlinear cloak designs.[115,146]

© 2012 WILEY-VCH Verlag GmbH & Co. KGaA, Weinheim

15214095, 2012, 44, Downloaded from https://onlinelibrary.wiley.com/doi/10.1002/adma.201202624 by Cochrane Russian Federation, Wiley Online Library on [13/02/2023]. See the Terms and Conditions (https://onlinelibrary.wiley.com/terms-and-conditions) on Wiley Online Library for rules of use; OA articles are governed by the applicable Creative Commons License

1521495, 2012, 44, Downloaded from https://onlinelibrary.wiley.com/doi/10.1002/adma.201202624 by Cochrane Russian Federation, Wiley Online Library on [13/02/2023]. See the Terms and Conditions (https://onlinelibrary.wiley.com/terms-and-conditions) on Wiley Online Library for rules of use; OA articles are governed by the applicable Creative Commons License

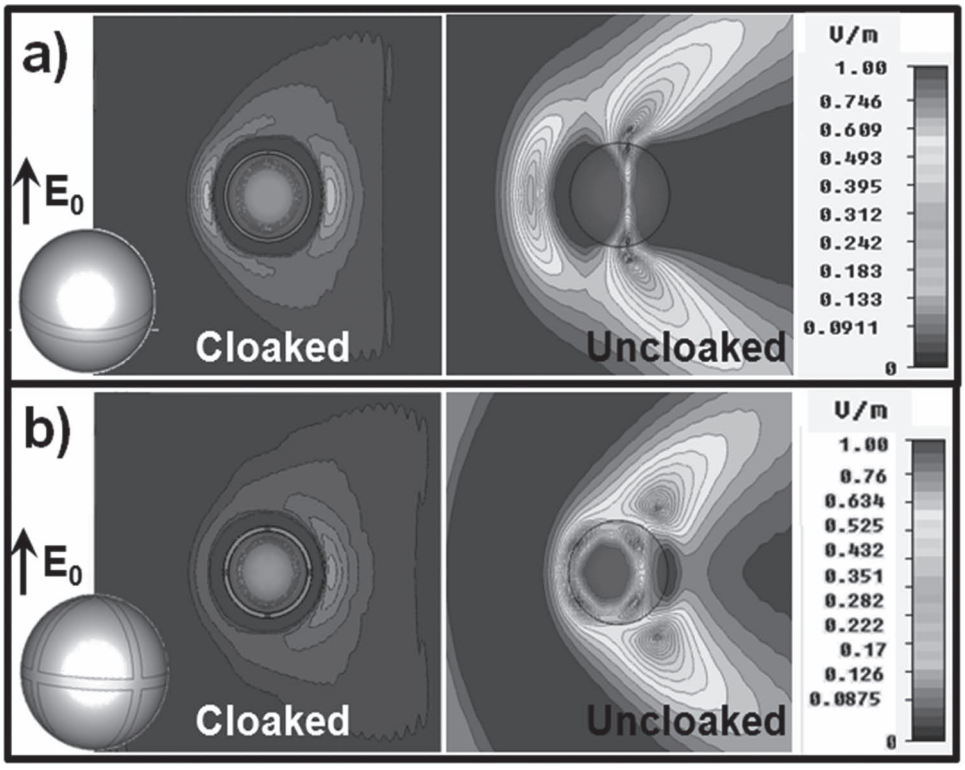

Figure 19. a) Left panel shows the amplitude of electric field on the H plane for a dielectric sphere covered with cloak 1 in Figure 12a, and right panel shows the uncloaked scenario. (b) is similar to (a), but for the cloak 2 design shown in Figure 12a.

5.4. Roadmap for Development of Scattering Cancellation Cloaks

In this section, we summarize the research and development roadmap for scattering-cancellation-based cloaks, based on the results reviewed in this paper, as shown in **Figure 20**. Each of these scattering-cancellation-based cloaks have different physical sizes and are particularly well suited for a specific spectral range, all being based on analogous phenomena of integral destructive interference of scattered fields for all directions. At RF and microwaves, mantle cloaks realized with low-cost and low-profile FSS and/or metasurface technology are particularly promising to realize cloaking devices. Also plasmonic cloaks are particularly robust, as the recent experimental realization for a 3D elongated object has shown.[45] In the near-infrared, visible and ultraviolet regions, instead of using metamaterials or structured surfaces, natural plasmonic materials may provide isotropic, low or negative real permittivity, and therefore may be ideal to realize plasmonic cloaking in these frequency ranges. Noble metals (i.e., silver, copper, aluminum or gold) can possess low or negative real permittivity at visible and UV frequencies, while some wide-bandgap semiconductors (i.e., gallium zinc oxide, aluminum zinc oxide or indium tin oxide) display the same properties in the infrared region.[7,8] In the frequency range between RF mantle cloaks realized with conducting metasurfaces and plasmonic cloaks in optics, graphene cloaks may be considered to realize the thinnest possible cloak at THz frequencies.[27,75,88,112,114] In this frequency range, there are no promising natural plasmonic materials that exhibit low or negative permittivity, with relatively low loss. Furthermore, it is rather difficult to pattern or synthesize an FSS and/or a metasurface, not to mention a bulk 3D metamaterial. We also highlight in the figure the nanocircuit-inspired cloak, well suited for the optical spectrum to connect the plasmonic and mantle cloaking approaches. In the future, new nanomaterial synthesis and nanofabrication methods may pave the way to more efficient cloaking methods, spanning the whole electromagnetic spectrum of interest. We envision that sensors or receivers cloaked by plasmonic and/or mantle layers may become a promising technology for low-noise and low-interference sensing and communication links, as already shown in a recent cloaked photodetector experiment.[34]

6. Conclusions

We have reviewed and outlined the most popular techniques employing metamaterials, metasurfaces, graphene and plasmonic materials to realize cloaking devices, with particular focus on scattering cancellation approaches. We have presented simulation and experimental results, highlighting their main features, analogies, and potentials, as well as physical insights into the involved physical mechanisms. We have also briefly reviewed other exciting cloaking techniques: the metamaterial cloaking based on transform optics rules, the transmission-line cloaking, and the metal-plate cloaking, underlying the main analogies, differences and advantages among these approaches.

© 2012 WILEY-VCH Verlag GmbH & Co. KGaA, Weinheim

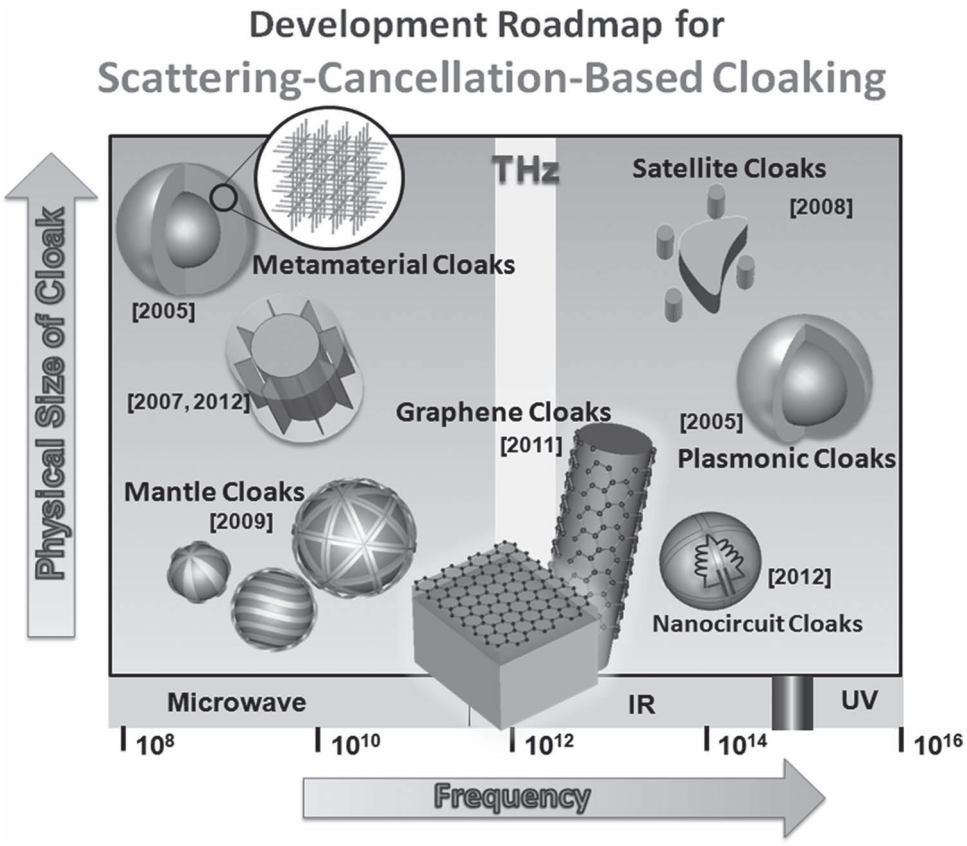

Figure 20. Research and development roadmap for scattering-cancellation-based cloaks. The plasmonic cloak using bulk metamaterial or plasmonic material was first proposed in 2005.[19] In 2007 plasmonic cloaks realized by parallel-plate metamaterial was proposed.[83] Cloaking by anti-phase plasmonic satellites surrounding the object, providing additional design flexibility was suggested in 2008.[93] In 2009, ultralow-profile mantle cloak based on the concept of cloaking by a surface was first proposed.[27] In 2011, the one-atom-thick graphene cloak was proposed for operation at THz frequencies.[114] We proposed in this paper the nanocircuit approach to mantle cloaking.

As in every technological innovation, each cloaking technique has its own advantages and disadvantages, challenging to be quantitatively analyzed and compared, and therefore each solution is feasible for specific applications and scenarios. Generally speaking, in an ideal scenario the transformation-based cloaks may outperform any other cloaking technique in terms of their capability to cloak large objects at the design frequency. However, they usually suffer from more severe bandwidth and sensitivity issues than scattering-cancellation cloaks, and the bandwidth limitations and the sensitivity to design imperfections grow exponentially with the size of the object to be cloaked. Recent papers have compared transformation and plasmonic cloaking techniques with respect to their bandwidth, feasible size, losses and frequency variations, showing that the plasmonic cloaking may outperform transformation-based cloaks for moderately-sized object (close to one wavelength).[146–147] Also, recent experiments have confirmed relatively broad bandwidths for 3D scattering-cancellation cloaks.[45] Mantle cloaks are particularly promising in this regard, as they combine the advantages of scattering cancellation approaches to easier realization, low profile and robustness to frequency and imperfections.

As today's nanomanufacturing and smart material technology continue to improve, we envision that in the near future invisibility cloaks realized with metamaterials, metasurfaces, and/or novel plasmonic materials will show numerous real-world applications ranging from RF and microwaves, to THz, infrared and optical frequencies, including not only camouflaging, but also noninvasive probing, biological and medical sensing and detection, high-quality near-field measurement, and low-interference communication and sensing networks. Active materials and non-Foster surfaces may further broaden the reach of cloaking technology by breaking fundamental limits, based on passivity and causality, in terms of bandwidth of operation. Besides, adding nonlinear loads, such as nonlinear optical materials or RF diodes, varactors and transistors, may enable tunable and switchable cloaking, which has been theoretically proposed for scattering-cancellation-based cloaks.[114,147–149]

Acknowledgements

This work was supported in part by the ONR MURI Grant No. N00014-10-1-0942 and by the National Science Foundation with CAREER award No. ECCS-0953311.

Received: June 29, 2012
Revised: August 29, 2012
Published online: October 19, 2012

© 2012 WILEY-VCH Verlag GmbH & Co. KGaA, Weinheim

15214095, 2012, 44, Downloaded from https://onlinelibrary.wiley.com/doi/10.1002/adma.201202624 by Cochrane Russian Federation, Wiley Online Library on [13/02/2023]. See the Terms and Conditions (https://onlinelibrary.wiley.com/terms-and-conditions) on Wiley Online Library for rules of use; OA articles are governed by the applicable Creative Commons License

15214095, 2012, 44, Downloaded from https://onlinelibrary.wiley.com/doi/10.1002/adma.201202624 by Cochrane Russian Federation, Wiley Online Library on [13/02/2023]. See the Terms and Conditions (https://onlinelibrary.wiley.com/terms-and-conditions) on Wiley Online Library for rules of use; OA articles are governed by the applicable Creative Commons License

REVIEW

[1] C. Caloz, T. Itoh, *Electromagnetic Metamaterials: Transmission Line Theory and Microwave Applications*, Wiley, New York **2005**.
[2] *Negative-Refraction Metamaterials* (Eds: G. V. Eleftheriades, K. G. Balmain), Wiley, New York **2005**.
[3] *Metamaterials: Physics and Engineering Explorations* (Eds: N. Engheta, R. W. Ziolkowski), Wiley, New York **2006**.
[4] A. K. Sarychev, V. M. Shalaev, *Electrodynamics of Metamaterials*, World Scientific, Singapore **2007**.
[5] R. Marques, F. Martin, M. Sorolla, *Metamaterials with Negative Parameters: Theory, Design and Microwave Applications*, Wiley, New York **2008**.
[6] P. R. West, S. Ishii, G. V. Naik, N. K. Emani, V. M. Shalaev, A. Boltasseva, *Laser Photonics Rev.* **2010**, *4*, 795.
[7] A. Boltasseva, H. A. Atwater, *Science* **2011**, *331*, 290.
[8] G. V. Naik, V. M. Shalaev, A. Boltasseva, *Proc. SPIE* **2010**, *7754*, 77540M.
[9] G. V. Naik, J. L. Schroeder, X. Ni, A. V. Kildishev, T. D. Sands, A. Boltasseva, *Opt. Express* **2012**, *2*, 478.
[10] S. H. Brewer, S. Franzen, *Chem. Phys.* **2004**, *300*, 285.
[11] F. Rana, *Nat. Nanotechnol.* **2011**, *6*, 611.
[12] F. Bonaccorso, Z. Sun, T. Hasan, A. C. Ferrari, *Nat. Photonics* **2010**, *4*, 611.
[13] J. B. Pendry, *Phys. Rev. Lett.* **2000**, *85*, 3966.
[14] R. A. Shelby, D. R. Smith, S. Schultz, *Science* **2001**, *292*, 77.
[15] W. Srituravanich, L. Pan, Y. Wang, C. Sun, D. B. Body, X. Zhang, *Nat. Nanotechnol.* **2008**, *3*, 733.
[16] X. Zhang, Z. Liu, *Nat. Mater.* **2008**, *7*, 435.
[17] A. Greenleaf, M. Lassas, G. Uhlmann, *Math. Res. Lett.* **2003**, *10*, 685.
[18] A. Alù, N. Engheta, *IEEE Trans. Antennas Propag.* **2003**, *51*, 2558.
[19] A. Alù, N. Engheta, *Phys. Rev. E* **2005**, *72*, 016623.
[20] G. W. Milton, N. A. Nicorovici, R. C. McPhedran, V. A. Podolskiy, *Proc. R. Soc. A* **2005**, *461*, 3999.
[21] J. B. Pendry, D. Schurig, D. R. Smith, *Science* **2006**, *312*, 1780.
[22] U. Leonhardt, *Science* **2006**, *312*, 1777.
[23] H. Chen, C. T. Chan, P. Sheng, *Nat. Mater.* **2010**, *9*, 387.
[24] V. M. Shalaev, *Science* **2008**, *322*, 384.
[25] A. Greenleaf, Y. Kurylev, M. Lassas, G. Uhlmann, *SIAM Rev.* **2009**, *51*, 3.
[26] U. Leonhardt, T. Tyc, *Science* **2009**, *323*, 110.
[27] A. Alù, *Phys. Rev. B* **2009**, *80*, 245115.
[28] A. Alù, N. Engheta, *Phys. Rev. Lett.* **2009**, *102*, 233901.
[29] A. Alù, N. Engheta, *Phys. Rev. Lett.* **2010**, *105*, 263906.
[30] A. Alù, N. Engheta, *Metamaterials* **2010**, *4*, 153.
[31] F. Bilotti, S. Tricarico, F. Pierini, L. Vegni, *Opt. Lett.* **2011**, *36*, 211.
[32] A. Greenleaf, Y. Kurylev, M. Lassas, G. Uhlmann, *Phys. Rev. E.* **2011**, *83*, 016603.
[33] X. Chen, G. Uhlmann, *Opt. Express* **2011**, *19*, 20518.
[34] P. Fan, U. K. Chettiar, L. Cao, F. Afshinmanesh, N. Engheta, M.L. Brongersma, *Nat. Photonics* **2012**, *6*, 380.
[35] Y. Hu, Y. Zhang, C. Xu, L. Lin, R. L. Snyder, Z. L. Wang, *Nano Lett.* **2011**, *11*, 2572.
[36] F. Gömöry, M. Solovyov, J. Šouc, C. Navau, J. Prat-Camps, A. Sanchez, *Science* **2012**, *335*, 1466.
[37] M. Farhat, S. Enoch, S. Guenneau, A. B. Movchan, *Phys. Rev. Lett.* **2008**, *101*, 134501.
[38] B. I. Popa, L. Zigoneanu, S. A. Cummer, *Phys. Rev. Lett.* **2011**, *106*, 253901.
[39] D. Schurig, J. J. Mock, B. J. Justice, S. A. Cummer, J. B. Pendry, A. F. Starr, D. R. Smith, *Science* **2006**, *314*, 977.
[40] B. Edwards, A. Alù, M. E. Young, M. Silveirinha, N. Engheta, *Phys. Rev. Lett.* **2008**, *100*, 033903.
[41] R. Liu, C. Ji, J. J. Mock, J. Y. Cui, D. R. Smith, *Science* **2009**, *323*, 366.
[42] P. Alitalo, F. Bongard, J. F. Zurcher, J. Mosig, S. A. Tretyakov, *J. Appl. Phys.* **2009**, *94*, 014103.
[43] S. A. Tretyakov, P. Alitalo, O. Luukkonen, C. Simovski, *Phys. Rev. Lett.* **2009**, *103*, 103905.
[44] D. Bao, K. Z. Rajab, Y. Hao, E. Kallos, W. Tang, C. Argyropoulos, Y. Piao, S. Yang, *New J. Phys.* **2011**, *13*, 103023.
[45] D. Rainwater, A. Kerkhoff, K. Melin, J.C. Soric, G. Moreno, A. Alù, *New J. Phys.* **2012**, *14*, 013051.
[46] P. Alitalo, A. E. Culhaoglu, A. V. Osipov, S. Thurner, E. Kemptner, S. A. Tretyakov, *J. Appl. Phys.* **2012**, *111*, 034901.
[47] W. Cai, U. K. Chettiar, A. V. Kildishev, V. M. Shalaev, *Nat. Photonics* **2007**, *1*, 224.
[48] J. Valentine, S. Zhang, T. Zentgraf, E. Ulin-Avila, D. A. Genov, G. Bartal, X. Zhang, *Nature* **2008**, *455*, 376.
[49] L. H. Gabrielli, J. Cardenas, C. B. Poitras, M. Lipson, *Nat. Photonics* **2009**, *3*, 461.
[50] T. M. Ergin, N. Stenger, P. Brenner, J. B. Pendry, M. Wegener, *Science* **2010**, *328*, 337.
[51] J. Renger, M. Kadic, G. Dupont, S. S. Acimovic, S. Guenneau, R. Quidant, S. Enoch, *Opt. Express* **2010**, *18*, 15757.
[52] B. Zhang, Y. Luo, X. Liu, G. Barbastathis, *Phys. Rev. Lett.* **2011**, *106*, 033901.
[53] X. Chen, Y. Luo, J. Zhang, K. Jiang, J. B. Pendry, S. Zhang, *Nat. Commun.* **2011**, *2*, 176.
[54] E. Semouchkina, D. H. Werner, G. B. Semouchkin, C. Pantano, *Appl. Phys. Lett.* **2010**, *96*, 233503.
[55] A. E. Aliev, Y. N. Garstein, R. Y. Baughman, *Nanotechnology* **2011**, *22*, 435704.
[56] H. Chen, B. I. Wu, B. Zhang, J. A. Kong, *Phys. Rev. Lett.* **2007**, *99*, 063903.
[57] H. Chen, X. Jiang, C. T. Chan, *Phys. Rev. B* **2007**, *76*, 241104.
[58] M. Yan, Z. Ruan, M. Qiu, *Phys. Rev. Lett.* **2007**, *99*, 233901.
[59] Z. Ruan, M. Yan, C. W. Neff, M. Qiu, *Phys. Rev. Lett.* **2007**, *99*, 113903.
[60] B. I. Popa, S. A. Cummer, *Phys. Rev. A* **2009**, *79*, 023806.
[61] N. Kundtz, D. Gaultney, D. R. Smith, *New J. Phys.* **2010**, *12*, 043039.
[62] S. A. Cummer, B. I. Popa, D. Schurig, D. R. Smith, *Phys. Rev. E.* **2006**, *74*, 036621.
[63] A. V. Kildishev, W. Cai, U. K. Chettiar, V. M. Shalaev, *New J. Phys.* **2008**, *10*, 115029.
[64] J. Li, J.B. Pendry, *Phys. Rev. Lett.* **2008**, *101*, 203901.
[65] E. Kallos, C. Argyropoulos, Y. Hao, *Phys. Rev. E.* **2009**, *79*, 063825.
[66] A. Alù, N. Engheta, *Phys. Rev. E.* **2008**, *78*, 045602(R).
[67] P. Alitalo, O. Luukkonen, L. Jylha, J. Venermo, S. A. Tretyakov, *IEEE Trans. Antennas Propag.* **2008**, *56*, 416.
[68] A. Alù, N. Engheta, *Opt. Express* **2007**, *15*, 7578.
[69] R. C. McPhedran, N. P. Nicorovici, L. C. Botten, G. W. Milton, *C.R. Phys.* **2009**, *10*, 391.
[70] M. Farhat, P. Y. Chen, S. Guenneau, S. Enoch, R. C. McPhedran, C. Rockstuhl, F. Lederer, *Phys. Rev. B* **2011**, *84*, 235105.
[71] E. Kallo, C. Argyropoulos, Y. Hao, A Alù, *Phys. Rev. B* **2011**, *84*, 045102.
[72] P. Alitalo, S. A. Tretyakov, *Phys. Rev. B* **2010**, *82*, 245111.
[73] C. A. Valagiannopoulos, P. Alitalo, *Phys. Rev. B* **2012**, *85*, 115402.
[74] A. Alù, D. Rainwater, A. Kerkhoff, *New J. Phys.* **2010**, *12*, 103028.
[75] A. Alù, N. Engheta, *Phys. Rev. Lett.* **2008**, *100*, 113901.
[76] H. Wang, X. Zhang, *J. Appl. Phys.* **2009**, *106*, 053302.
[77] C. H. Papas, *Theory of Electromagnetic Wave Propagation*, Dover Publications, New York **1988**.
[78] *Handbook of Mathematical Functions With Formulas, Graphs, and Mathematical Tables* (Eds: M. Abramowitz, I. A. Stegun)Dover, New York **1972**.
[79] C. F. Bohren, D. R. Huffman, *Absorption and Scattering of Light by Small Particles*, Wiley, New York **1998**.

© 2012 WILEY-VCH Verlag GmbH & Co. KGaA, Weinheim

[80] F. Bilotti, S. Tricarico, L. Vegni, *New J. Phys.* **2008**, *10*, 115035.
[81] A. Alù, N. Engheta, *Opt. Express* **2007**, *15*, 3318.
[82] H. A. Yousif, R. E. Mattis, K. Kozminski, *Appl. Opt.* **1994**, *33*, 4013.
[83] C. A. Balanis, *Advanced Engineering Electromagnetics*, Wiley, New York **1989**.
[84] M. Silveirinha, A. Alù, N. Engheta, *Phys. Rev. E* **2007**, *75*, 036603.
[85] J. Soric, N. Engheta, S. Maci, A. Alù, IEEE Trans. Antennas Propag. DOI: 10.1109/TAP.2012.2214994.
[86] CST Microwave Studio 2011, http://www.cst.com (last accessed September 2012).
[87] Cuming Microwave, http://cumingmicrowave.com (last accessed September 2012).
[88] M. Silveirinha, A. Alù, N. Engheta, *Phys. Rev. B* **2008**, *78*, 075107.
[89] S. Muhlig, M. Farhat, C. Rockstuhl, F. Lederer, *Phys. Rev. B* **2011**, *83*, 195116.
[90] A. Monti, F. Bilotti, A. Toscano, *Opt. Lett.* **2011**, *36*, 4479.
[91] S. Tricarico, F. Bilotti, L. Vegni, *J. Eur. Opt. Soc.* **2009**, *4*, 09021.
[92] F. Bilotti, S. Tricarico, L. Vegni, *IEEE Trans. Nanotechnol.* **2010**, *9*, 55.
[93] M. Silveirinha, A. Alù, N. Engheta, *Phys. Rev. B* **2008**, *78*, 205109.
[94] Y. Gao, J. P. Huang, K. W. Yu, *J. Appl. Phys.* **2009**, *105*, 124505.
[95] A. E. Serebryannikov, Ekmel Ozbay, *J. Opt. A: Pure Appl. Opt.* **2009**, *11*, 114020.
[96] A. E. Serebryannikov, P. V. Usik, Ekmel Ozbay, *Opt. Express* **2009**, *17*, 16869.
[97] R. F. Harrington, *Proc. IEEE* **1964**, *111*, 617.
[98] W. K. Kahn, H. Kurss, *IEEE Trans. Antennas Propag.* **1965**, *13*, 671.
[99] R. B. Green, *IEEE Trans. Antennas Propag.* **1966**, *14*, 17.
[100] R. C. Hansen, *Proc. IEEE* **1989**, *77*, 659.
[101] J. B. Andersen, A. Frandsen, *IEEE Trans. Antennas Propag.* **2005**, *53*, 2843.
[102] D. H. Kwon, D. M. Pozar, *IEEE Trans. Antennas Propag.* **2009**, *57*, 3720.
[103] A. Alù, S. Maslovski, *IEEE Trans. Antennas Propag.* **2010**, *58*, 1436.
[104] A. O. Karilainen, S. A. Tretyakov, *IEEE Trans. Antennas Propag. Mag.* **2012**, *60*, 3471.
[105] D. S. Filonov, A. P. Slobozhanyuk, P. A. Belov, Y. S. Kivshar, *Phys. Status Solidi RRL* **2012**, *6*, 46.
[106] S. Tricarico, F. Bilotti, A. Alù, L. Vegni, *Phys. Rev. E* **2010**, *81*, 026602.
[107] M. D. Guild, M. Haberman, A. Alù, *Wave Motion* **2011**, *48*, 468.
[108] M. D. Guild, M. Haberman, A. Alù, *J. Acoust. Soc. Am.* **2011**, *129*, 1355.
[109] B. A. Munk, *Frequency Selective Surface: Theory and Design*, Wiley, New York **2000**.
[110] P. Alitalo, H. Kettunen, S. A. Tretyakov, *J. Appl. Phys.* **2010**, *107*, 034905.
[111] P. Y. Chen, A. Alù, Presented at *IEEE Int. Sym. Antennas Propag.*, 11–17 July 2010.
[112] P. Y. Chen, A. Alù, *Phys. Rev. B* **2011**, *84*, 205110.
[113] P. Y. Chen, F. Monticone, A. Alù, *IEEE Antennas Propag. Lett.* **2011**, *5*, 1598.
[114] P. Y. Chen, A. Alù, *ACS Nano* **2011**, *5*, 5855.
[115] R. M. Foster, *Bell Syst. Tech. J.* **1924**, *3*, 259.
[116] S. Hrabar, I. Krois, A. Kiricenko, *Metamaterials* **2009**, *4*, 89.
[117] S. Hrabar, I. Krois, I. Bonic, A. Kiricenko, *Appl. Phys. Lett.* **2011**, *99*, 254103.
[118] Y. R. Padooru, A. B. Yakovlev, C. S. R. Kaipa, F. Medina, F. Mesa, *Phys. Rev. B* **2011**, *84*, 035108.
[119] C. S. R. Kaipa, A. B. Yakovlev, F. Medina, F. Mesa, C. A. M. Butler, P. Alastair, *Opt. Express* **2010**, *18*, 13309.
[120] Y. R. Padooru, A. B. Yakovlev, P. Y. Chen, A. Alù, *J. Appl. Phys.* **2012**, *112*, 034907.
[121] P. Y. Chen, C. H. Chen, H. Wang, J. H. Tsai, W. X. Ni, *Opt. Express* **2008**, *17*, 12806.
[122] D. J. Kern, D. H. Werner, A. Monorchio, L. Lanuzza, M. J. Wilhelm, *IEEE Trans. Antennas Propag.* **2005**, *53*, 8.
[123] A. K. Geim, K. S. Novoselov, *Nat. Mater.* **2007**, *6*, 183.
[124] Y. M. Lin, K. A. Jenkins, A. Valdes-Garcia, J. P. Small, D. B. Farmer, P. Avouris, *Nano Lett.* **2009**, *9*, 422.
[125] K. I. Bolotin, K. J. Sikesbianga, M. Klimac, G. Fudenberga, J. Honec, P. Kima, H. L. Stormera, *Solid State Commun.* **2008**, *145*, 351.
[126] F. Rana, *IEEE Trans. Nanotechnol.* **2008**, *7*, 91.
[127] G. W. Hanson, *J. Appl. Phys.* **2006**, *103*, 064302.
[128] A. Vakil, N. Engheta, *Science* **2011**, *332*, 1291.
[129] M. Jablan, H. Buljan, M. Sojačić, *Phys. Rev. B* **2009**, *80*, 245435.
[130] L. Ju, B. Geng, J. Horng, C. Girit, M. Martin, Z. Hao, H. A. Bechtel, X. Liang, A. Zettl, Y. R. Shen, Feng Wang, *Nat. Nanotechnol.* **2011**, *6*, 630.
[131] J. Chen, M. Badioli, P. Alonso-González, S. Thongrattanasiri, F. Huth, J. Osmond, M. Spasenovi , A. Centeno, A. Pesquera, P. Godignon, A. Z. Elorza, N. Camara, F. J. García de Abajo, R. Hillenbrand, F. H. L. Koppens, *Nature* **2012**, *487*, 77.
[132] V. P. Gusynin, S. G. Sharapov, J. P. Carbotte, *J. Phys.: Condens. Matter* **2007**, *19*, 026222.
[133] G. W. Hanson, *IEEE Trans. Antennas Propag.* **2008**, *56*, 747.
[134] R. Nair, R. P. Blake, A. N. Grigorenko, K. S. Novoselov, T. J. Booth, T. Stauber, N. M. R. Peres, A. K. Geim, *Science* **2008**, *320*, 1308.
[135] F. T. Chuang, P. Y. Chen, T. C. Cheng, C. H. Chien, B. J. Li, *Nanotechnology* **2007**, *18*, 395702.
[136] D. Mann, A. Javey, J. Kong, Q. Wang, H. Dai, *Nano Lett.* **2003**, *3*, 1541.
[137] J. Q. Hu, Y. Bando, F. Xu, Y. Li, J. Zhan, J. Xu, D. Golberg, *Adv. Mater.* **2004**, *16*, 153.
[138] G. Bhimarasetti, J. M. Cowley, M. K. Sunkara, *Nanotechnology* **2005**, *16*, S362.
[139] R. Wang, Y. Hao, Z. Wang, H. Gong, J. T. L. Thong, *Nano Lett.* **2010**, *10*, 4844.
[140] N. Engheta, *Science* **2007**, *317*, 5845.
[141] N. Engheta, A. Salandrino, A. Alù, *Phy. Rev. Lett.* **2005**, *95*, 095504.
[142] A. Alù, M. Young, N. Engheta, *Phys. Rev. B* **2008**, *77*, 144107.
[143] Y. Sun, B. Edwards, A. Alù, N. Engheta, *Nat. Mater.* **2012**, *11*, 208.
[144] P. B. Johnson, R. W. Christy, *Phys. Rev. B* **1972**, *6*, 4370.
[145] A. Alù, M. Young, N. Engheta, *Phys. Rev. B* **2008**, *77*, 144107.
[146] P. Y. Chen, A. Alù, *Phys. Rev. B* **2010**, *82*, 235405.
[147] C. Argyropoulos, P. Y. Chen, F. Monticone, G. D'Aguanno, A. Alù, *Phys. Rev. Lett.* **2012**, *108*, 263905.
[148] P. Li, Y. Liu, Y. Meng, *Opt. Express* **2010**, *18*, 12646.
[149] P. Li, Y. Liu, Y. Meng, M. Zhu, *J. Phys. D: Appl. Phys.* **2010**, *43*, 175404.

© 2012 WILEY-VCH Verlag GmbH & Co. KGaA, Weinheim

15214095, 2012, 44, Downloaded from https://onlinelibrary.wiley.com/doi/10.1002/adma.201202624 by Cochrane Russian Federation, Wiley Online Library on [13/02/2023]. See the Terms and Conditions (https://onlinelibrary.wiley.com/terms-and-conditions) on Wiley Online Library for rules of use; OA articles are governed by the applicable Creative Commons License